Cell Reports

Report

In Vivo Estimates of Liver Metabolic Flux Assessed by ^{13}C-Propionate and ^{13}C-Lactate Are Impacted by Tracer Recycling and Equilibrium Assumptions

Graphical Abstract

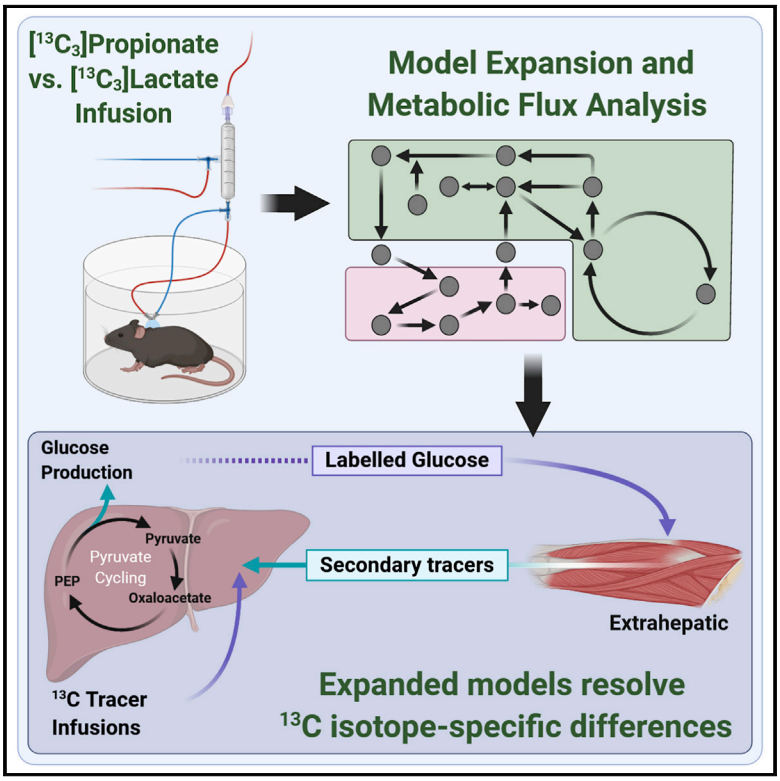

Authors

Clinton M. Hasenour, Mohsin Rahim, Jamey D. Young

Correspondence

j.d.young@vanderbilt.edu

In Brief

Prior studies of *in vivo* liver metabolism using ^{13}C tracers have produced divergent estimates of Krebs cycle and anaplerotic fluxes. Hasenour et al. present findings that are critical for interpreting experiments with two widely used metabolic tracers and introduce modeling strategies to improve isotope-based determination of liver metabolic fluxes.

Highlights

- Secondary tracers and incomplete equilibration influence *in vivo* flux estimates
- Liver pyruvate cycle flux is affected by assumptions vis-à-vis Cori cycle activity
- Expanded models resolve ^{13}C tracer-specific differences in hepatic fluxes
- ^{13}C lactate and propionate tracers indicate significant liver pyruvate cycling

Hasenour et al., 2020, Cell Reports *32*, 107986
August 4, 2020
https://doi.org/10.1016/j.celrep.2020.107986

CellPress

Cell Reports

CellPress
OPEN ACCESS

Report

In Vivo Estimates of Liver Metabolic Flux Assessed by ^{13}C-Propionate and ^{13}C-Lactate Are Impacted by Tracer Recycling and Equilibrium Assumptions

Clinton M. Hasenour,[1,3] Mohsin Rahim,[1,3] and Jamey D. Young[1,2,4,*]
[1]Department of Chemical and Biomolecular Engineering, Vanderbilt University, Nashville, TN 37235, USA
[2]Department of Molecular Physiology and Biophysics, Vanderbilt University, Nashville, TN 37235, USA
[3]These authors contributed equally
[4]Lead Contact
*Correspondence: j.d.young@vanderbilt.edu
https://doi.org/10.1016/j.celrep.2020.107986

SUMMARY

Isotope-based assessment of metabolic flux is achieved through a judicious balance of measurements and assumptions. Recent publications debate the validity of key assumptions used to model stable isotope labeling of liver metabolism *in vivo*. Here, we examine the controversy surrounding estimates of liver citric acid cycle and gluconeogenesis fluxes using a flexible modeling platform that enables rigorous testing of standard assumptions. Fasted C57BL/6J mice are infused with [$^{13}C_3$]lactate or [$^{13}C_3$]propionate isotopes, and hepatic fluxes are regressed using models with gradually increasing complexity and relaxed assumptions. We confirm that liver pyruvate cycling fluxes are incongruent between different ^{13}C tracers in models with conventional assumptions. When models are expanded to include more labeling measurements and fewer constraining assumptions, however, liver pyruvate cycling is significant, and inconsistencies in hepatic flux estimates using [$^{13}C_3$]lactate and [$^{13}C_3$]propionate isotopes emanate, in part, from peripheral tracer recycling and incomplete isotope equilibration within the citric acid cycle.

INTRODUCTION

Hepatic gluconeogenesis and the mitochondrial citric acid cycle (CAC) act in concert to supply the body with glucose when the dietary supply is reduced (e.g., during fasting). Many reactions in these pathways are catalyzed by regulatory enzymes that have been proposed as drug targets for treating insulin resistance, type 2 diabetes, and fatty liver disease. There has been a long-running debate regarding the nature of liver metabolic adaptations that occur during progression of these obesity-related conditions. Some groups hypothesize that impairments in mitochondrial metabolism are responsible for accumulation of toxic lipid species that cause insulin resistance and tissue damage in the liver. Others hypothesize that hepatic lipid overload causes elevations in CAC and anaplerotic fluxes that drive excess gluconeogenesis and accumulation of toxic free radicals. Because metabolic flux alterations cannot be assessed *in vivo* without isotope tracers, the two competing hypotheses cannot be completely resolved without accurate methods to model and interpret data from *in vivo* isotope labeling experiments (ILEs).

An ILE introduces a stable or radioactive tracer (e.g., containing heavy isotopes such as ^{13}C or ^{14}C) to a live biological system. After the tracer has been sufficiently metabolized through the target biochemical pathways of interest, the isotope enrichment of downstream metabolites is determined experimentally. Because different pathways rearrange the labeled atoms in unique ways, it is often possible to calculate metabolic flux rates from the relative abundance of different isotopically labeled species (i.e., isotopomers) comprising those metabolites. Various approaches have been taken to estimate hepatic pathway fluxes from *in vivo* ILEs. Least-squares regression approaches have been developed to estimate fluxes from metabolite mass isotopomer distributions (MIDs). Other approaches relate positional isotopomer abundances to pathway fluxes through distilled mathematical equations.

Regardless of the approach, assumptions are implemented to limit the complexity of model-based flux analysis. It is often assumed that primary isotopes equilibrate completely in the liver; also, the release, circulation, and reuptake of enriched products of liver metabolism are assumed to have a negligible effect on liver metabolic flux estimates. A challenge to these assumptions was illustrated in the classic debate over *in vivo* estimates of the parameter *y*, which represents the ratio of liver anaplerosis to citrate synthase flux. In the academic exchange, studies that used isotopic acetate or lactate yielded very different flux ratios. This incompatibility was partially reconciled by evidence showing that, in contrast to lactate, the extensive extrahepatic metabolism of isotopic acetate generated metabolites that artifactually lowered *y* values (Beylot et al., 1995; Katz et al., 1993; Landau, 1991; Landau et al., 1993; Schumann et al., 1991).

The aforementioned studies underscore the importance of secondary sites of isotope metabolism and generation. We

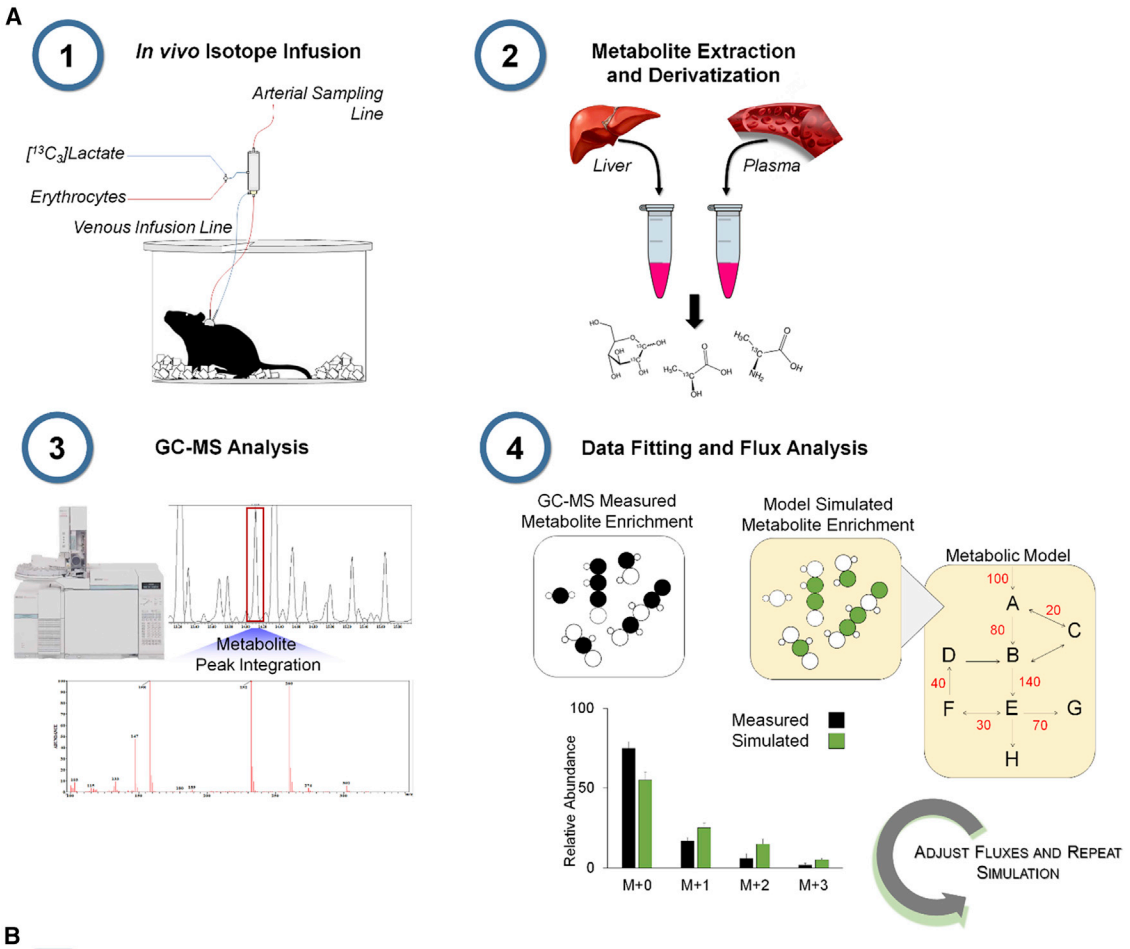

(legend on next page)

previously developed a modeling platform for *in vivo* liver metabolic flux analysis (MFA) that has been optimized for application to the conscious mouse (Hasenour et al., 2015; Figure 1A). Mice are infused with ^{2}H and/or ^{13}C isotopes, metabolites are analyzed by gas chromatography-mass spectrometry (GC-MS), and fluxes are estimated by least-squares regression of MID measurements using the Isotopomer Network Compartmental Analysis (INCA) software (Young, 2014). One advantage of INCA is that users can adjust the mathematical model to rapidly test the effects of specific reactions or modeling assumptions on the best-fit solution (Figure 1B). Nevertheless, our MFA platform shares some common challenges with other contemporary *in vivo* flux analysis approaches. Specifically, stable isotopes delivered in mass quantities may perturb the intrinsic metabolism of the pathways they are intended to assess. Primary isotopes or their enriched products may also be metabolized in non-target tissues *in vivo*, and metabolites enriched from their breakdown or exchange may circulate to the liver and further affect flux estimates.

Here we applied INCA to model the formation and effects of secondary tracers on liver flux analysis *in vivo*. These effects were tested in models that treat the liver as a single compartment or as a central hub in a multi-compartment network that accommodates the Cori cycle. Fluxes were regressed in models constrained by more common assumptions (base models) or expanded to rigorously account for incomplete isotope equilibration and additional metabolite measurements (expanded models). Using the aforementioned models, we assessed differences in the utility of [$^{13}C_3$]propionate ($^{13}C_3$Prop) and [$^{13}C_3$] lactate ($^{13}C_3$Lac) as tracers for regressing liver metabolic fluxes, with or without ^{2}H isotopes, in overnight-fasted C57BL/6J mice.

RESULTS

Secondary Tracer Effects Influence Estimates of Liver Pyruvate Cycling

We previously described a base model of *in vivo* liver metabolism that was applied to regress hepatic CAC and gluconeogenic fluxes from MID measurements of plasma glucose obtained from conscious, unrestrained mice (Hasenour et al., 2015). The model consists of a biochemical network with hydrogen and carbon atom transitions defined for each reaction (Table S1). The model assumes full equilibration of four-carbon (4C) intermediates in the CAC and no re-entry of labeled CO_2 or other secondary tracers. We used the best-fit solutions obtained from our prior studies of four long-term fasted mice infused with $^{13}C_3$Prop/^{2}H tracers to simulate the predicted MIDs of liver lactate (Lac261) and alanine (Ala260) fragment ions (Figure 2A). The simulated MIDs qualitatively resembled the measured enrichments of liver lactate and alanine, confirming that the base model is capable of accurately predicting isotope enrichments in other liver-derived metabolites in addition to glucose.

The assumption that secondary tracer effects are minimal is a pragmatic first approximation because analyzing sources of secondary tracers and deriving equations that account for those measurements *ad hoc* may be impractical in some cases. However, upon further investigation, we found that plasma lactate and urea (an indicator of circulating bicarbonate) were enriched significantly above the natural isotopic background following 120 min of $^{13}C_3$Prop/^{2}H infusion (Figure 2B). Inclusion of these measured lactate and CO_2 enrichments in the model regressions (Figure 2C) increased pyruvate cycling flux estimates ($V_{PC.L}$, $V_{PCK.L}$, and $V_{PK+ME.L}$[see MFA Model Terminology in the STAR Methods]) in the liver (Figures 2D and S1A), similar to the effect of $^{14}CO_2$ recycling in prior studies using [3-^{14}C]lactate in humans (Magnusson et al., 1991). In summary, these findings indicate that recycling of labeled lactate and CO_2 to the liver from the plasma is significant and that it likely affects *in vivo* estimates of liver pyruvate cycling obtained with ^{13}C tracers when applying the assumptions implicit to our base model.

Incongruent Hepatic Flux Estimates Are Obtained with Base Models of $^{13}C_3$Lac/^{2}H and $^{13}C_3$Prop/^{2}H Tracers

Adjustments were made to the base model of liver metabolism to accommodate a study with infusion of $^{13}C_3$Lac/^{2}H or $^{13}C_3$Prop/^{2}H isotopes (Table S1). The infusion rate for each ^{13}C isotope was analogous to previous studies (Hasenour et al., 2015; Perry et al., 2016). All mice were long term fasted to induce a gluconeogenic state of the liver. No differences in glucose-producing fluxes or blood glucose concentrations were observed between $^{13}C_3$Lac/^{2}H and $^{13}C_3$Prop/^{2}H tracer infusions (Figures 2E, 2F, S1B, and S2A). Nevertheless, pyruvate cycle fluxes ($V_{PC.L}$, $V_{PCK.L}$, and $V_{PK+ME.L}$) estimated from $^{13}C_3$Prop/^{2}H infusions were higher than those estimated with an analogous model of $^{13}C_3$Lac/^{2}H infusion (Figures 2E, S1B, and S2A; Table S2). Thus, best-fit pyruvate cycle fluxes obtained from base models were incongruent between $^{13}C_3$Lac/^{2}H and $^{13}C_3$Prop/^{2}H labeling studies.

A similar disparity has been observed in perfused livers (Satapati et al., 2015) and *in vivo* (Perry et al., 2016). Others have proposed that these discrepancies may result from incomplete randomization of ^{13}C atoms derived from ^{13}C-lactate because of its lesser interconversion with symmetric 4C intermediates in the CAC. This is purported to occur for ^{13}C tracers that enter the CAC downstream of fumarate (e.g., lactate or alanine) rather than those that enter upstream of succinate (e.g., propionate)

Figure 1. Metabolic Flux Analysis (MFA) Determines Fluxes through Model-Based Regression of Isotope Labeling Measurements

(A) MFA workflow. (1) Stable isotopes and replacement erythrocytes are infused intravenously into catheterized mice to enrich liver and plasma metabolites. (2) Plasma and liver tissue harvested at the end of the infusion are extracted and derivatized for GC-MS analysis. (3) Chromatographic peaks corresponding to the metabolites of interest are integrated and processed to obtain mass isotopomer distributions (MIDs). (4) The best-fit solution for all fluxes included in the metabolic model is obtained by minimizing the sum of squared residuals (SSR) between experimentally determined and model-simulated MIDs.

(B) Verification of the best-fit solution. (1) The best-fit solution for each mouse is accepted when the minimized SSR is within the expected range of a chi-square cumulative distribution function. (2) Flux uncertainties are assessed by determining the sensitivity of the minimized SSR to variations in each flux value. For example, the points of intersection with the dotted line indicate the boundaries of the 95% confidence interval (CI) of the estimated pyruvate carboxylase (PC) flux. (3) Varying the flux values away from the optimal solution increases the measurement residuals, as shown in the suboptimal case.

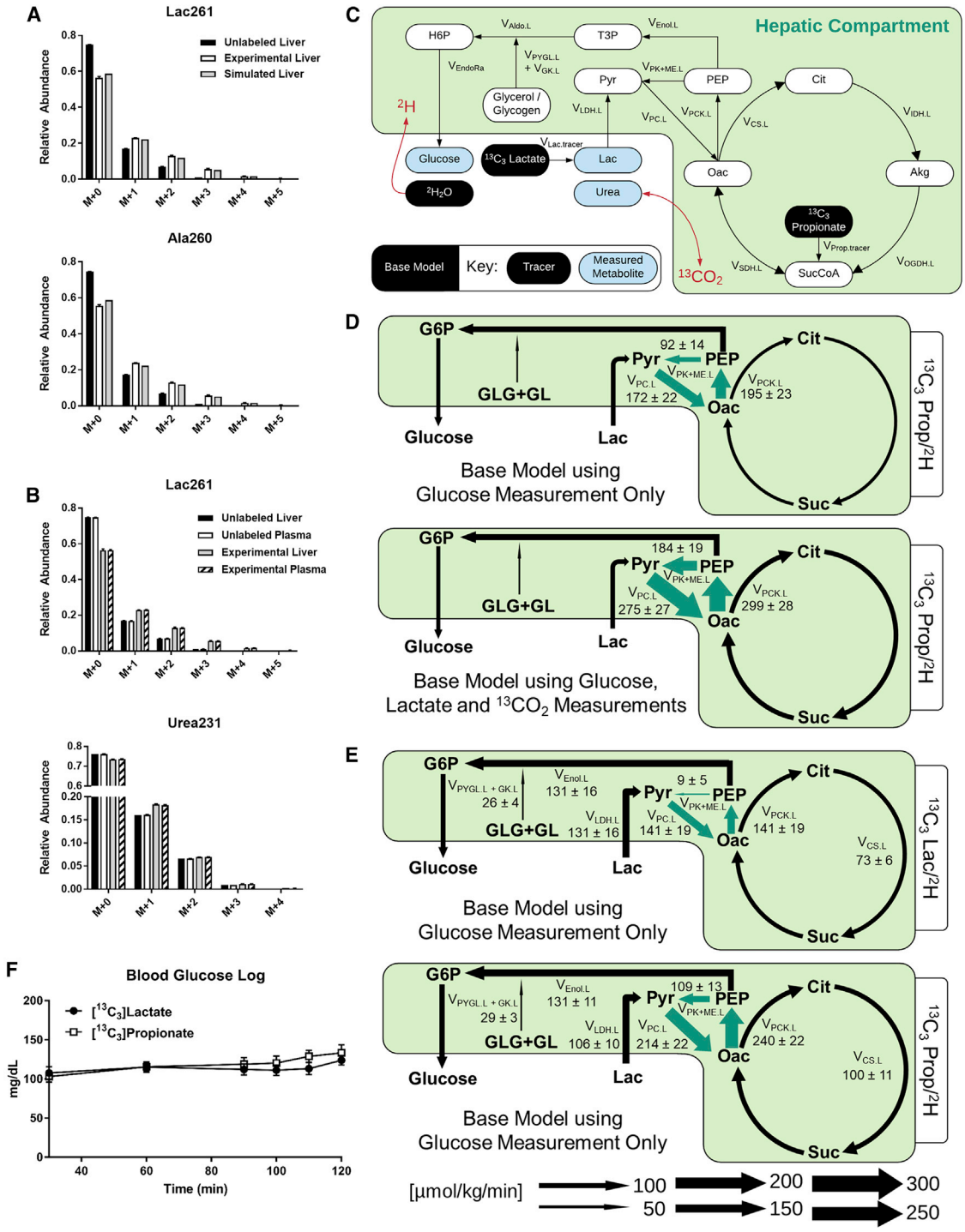

Figure 2. The Base Model Shows Evidence of Secondary Tracer Effects and Provides Different Estimates of Hepatic Fluxes for $^{13}C_3$Lac/^{2}H and $^{13}C_3$Prop/^{2}H Tracers

(A) Model-simulated and empirically measured (means ± SEM, n = 4) liver metabolite MIDs for lactate (mass-to-charge ratio [*m/z*] 261) and alanine (*m/z* 260).

(B) MIDs of plasma and liver lactate (*m/z* 261) and urea (*m/z* 231) obtained at isotopic steady state from long-term fasted C57BL/6J mice infused with $^{13}C_3$Prop/^{2}H isotopes contrasted with MIDs from unlabeled control samples (means ± SEM, n = 4).

(C) Network map of the base model showing infusion of $^{13}C_3$Lac or $^{13}C_3$Prop with $^{2}H_2O$. Plasma urea was used as a proxy measurement for CO_2 enrichment.

(D) Flux estimates obtained from the base model using plasma glucose enrichments alone contrasted with those that included $^{13}CO_2$ and plasma lactate measurements in the flux regression. Arrows highlighted in green represent significant changes between flux estimates obtained from the base model using the two measurement sets. Fluxes are expressed as means ± SEM (n = 4, *p ≤ 0.05).

(legend continued on next page)

(Satapati et al., 2015). Thus, we next examined the effects of incomplete isotope randomization on estimated flux ratios in our base models.

$^{13}C_3$Lac Infusion without ^{2}H Tracers Enables Rigorous Testing of Base Model Assumptions

Because of the aforementioned uncertainties related to (1) the extent of reversibility of 4C reactions of the CAC and (2) the influence of secondary tracer recycling on liver flux estimates, we designed a study to specifically address these assumptions by infusing mice with $^{13}C_3$Lac only (Figures 1A and 3A), without interference from ^{2}H tracers. Our measurement set was expanded to include additional plasma and liver metabolites not typically considered in prior *in vivo* flux analyses: lactate and alanine from both liver and plasma and glutamate, alpha-ketoglutarate, aspartate, and urea extracted from liver tissue.

Infusion of $^{13}C_3$Lac significantly increased the enrichment of circulating and hepatic metabolites (Figure S3). We observed significant M+1 and M+2 enrichments of liver alanine (Figure 3B) and plasma lactate (Figure 3C) after correcting the MIDs for natural background abundance of stable isotopes. The presence of these mass isotopomers reflects contributions from liver pyruvate cycling and extrahepatic Cori cycling. The abundance of recycled M+1 and M+2 isotopomers relative to the uncycled M+3 isotopomer is higher in liver alanine than in plasma lactate, indicating that intrahepatic pyruvate cycling occurs after lactate is extracted from plasma. The presence of M+1 and M+2 isotopomers in plasma lactate also provides some evidence that tracer recycling occurs outside of the liver, and the contribution from Cori cycling should be considered when making quantitative estimates of liver pyruvate cycle fluxes.

Next we examined measurements of liver oxaloacetate labeling to assess the randomization of M+3 species that traverse the 4C reactions of the CAC (Figure 3D). The measured M+3 and M+4 abundances of the Asp418 fragment ion (Figure 3E), which is biosynthetically derived from oxaloacetate, and the M+3 abundance of Asp390 (Figure S3A), which is derived from carbons 2–4 of oxaloacetate, were used to calculate the fractional abundances of the Oac_{1110} and Oac_{0111} isotopomers (STAR Methods). After accounting for $^{13}CO_2$ recycling, randomization in the oxaloacetate pool was determined to be ~90% with $^{13}C_3$Lac as a tracer (Figure 3F). A similar calculation can be performed with predicted Ala and Asp MIDs simulated from the base model of liver metabolism; a model that accounts for $^{13}CO_2$ recycling and assumes 90%, but not 100%, randomization leads to results comparable with those derived from the empirically measured MIDs (Figure 3F). These results suggest that *in vivo* estimates of hepatic metabolism would benefit from relaxing common assumptions regarding secondary tracer recycling and equilibration of 4C intermediates in the CAC.

Model Expansion to Account for Extrahepatic Metabolism Significantly Alters Pyruvate Cycle and CAC Fluxes

To relax several constraining assumptions of the base model and accommodate a broader set of plasma and tissue measurements, we constructed an expanded model that explicitly accounts for Cori cycling between hepatic and extrahepatic compartments (Figure 4A; Table S3). Liver pyruvate was allowed to reversibly exchange with liver lactate/alanine and glutamate was allowed to reversibly exchange with α-ketoglutarate. Importantly, the triose phosphate isomerase (TPI) and fumarate hydratase (FH) reactions were no longer assumed to fully equilibrate; instead, the reaction reversibilities were treated as adjustable parameters and determined by model regression of plasma and tissue MIDs. When the expanded model was regressed to data from $^{13}C_3$Lac infusions, the best-fit flux estimates indicated that the FH reaction was ~92% equilibrated, matching closely values determined empirically from analysis of oxaloacetate isotopomer ratios (Figure 3F). Because mice were fasted to deplete liver glycogen prior to isotope infusions, the regressed estimates of glucose production from glycogen were typically ~1%. Thus, flux from glycogen to G6P in liver ($V_{PYGL.L}$) was treated as inactive in the subsequent analyses to improve model reproducibility.

We compared best-fit solutions obtained from one-compartment (i.e., liver only) or two-compartment versions of the expanded model when regressed with plasma and liver MIDs obtained from $^{13}C_3$Lac infusions (Figures 4B and S4). Model expansion did not adversely affect flux precision as the confidence intervals for most fluxes were well constrained in both models (Figures S5A and S5B). Liver glucose production and net lactate uptake fluxes were not significantly different between the two models. Gluconeogenesis from phosphoenolpyruvate (PEP) accounted for the majority of endogenous glucose production (V_{EndoRa}), with a smaller fraction emanating from glycerol, and total liver cataplerotic/anaplerotic flux ($V_{PCK.L}$) was ~4-fold higher than the rate of citrate synthase ($V_{CS.L}$) in both models (Figures 4B and S4). In contrast, allowing return of lactate through the Cori cycle reduced liver pyruvate cycling ($V_{PK+ME.L}$, $V_{PC.L}$, and $V_{PCK.L}$) and CAC ($V_{CS.L}$) fluxes in the two-compartment model relative to the liver-only model (Figure 4B). Nevertheless, liver pyruvate cycling remained substantial in both models, with ~57% of total anaplerosis returned to pyruvate ($V_{PK+ME.L}$) in the two-compartment model compared with ~68% in the liver-only model (Figure 4B).

Pyruvate decarboxylation by the pyruvate dehydrogenase (PDH) complex is generally assumed to be low under long-term-fasted conditions. Although less precise, fluxes regressed using one- or two-compartment expanded models with an active PDH reaction were consistent with low levels of pyruvate decarboxylation ($V_{PDH.L}$ was ~5% the rate of total

(E) Flux estimates obtained from the base model using plasma glucose enrichments alone in mice infused with $^{13}C_3$Lac/^{2}H or $^{13}C_3$Prop/^{2}H isotopes. Arrows highlighted in green show significant flux changes between the $^{13}C_3$Lac/^{2}H and $^{13}C_3$Prop/^{2}H isotope studies using the base model. Fluxes are expressed as means ± SEM (n = 6–7, *p ≤ 0.05).

(F) Blood glucose log (milligrams per deciliter) during infusion of $^{13}C_3$Lac/^{2}H or $^{13}C_3$Prop/^{2}H isotopes in 19- to 20-h-fasted C57BL/6J mice (means ± SEM, n = 6–7).

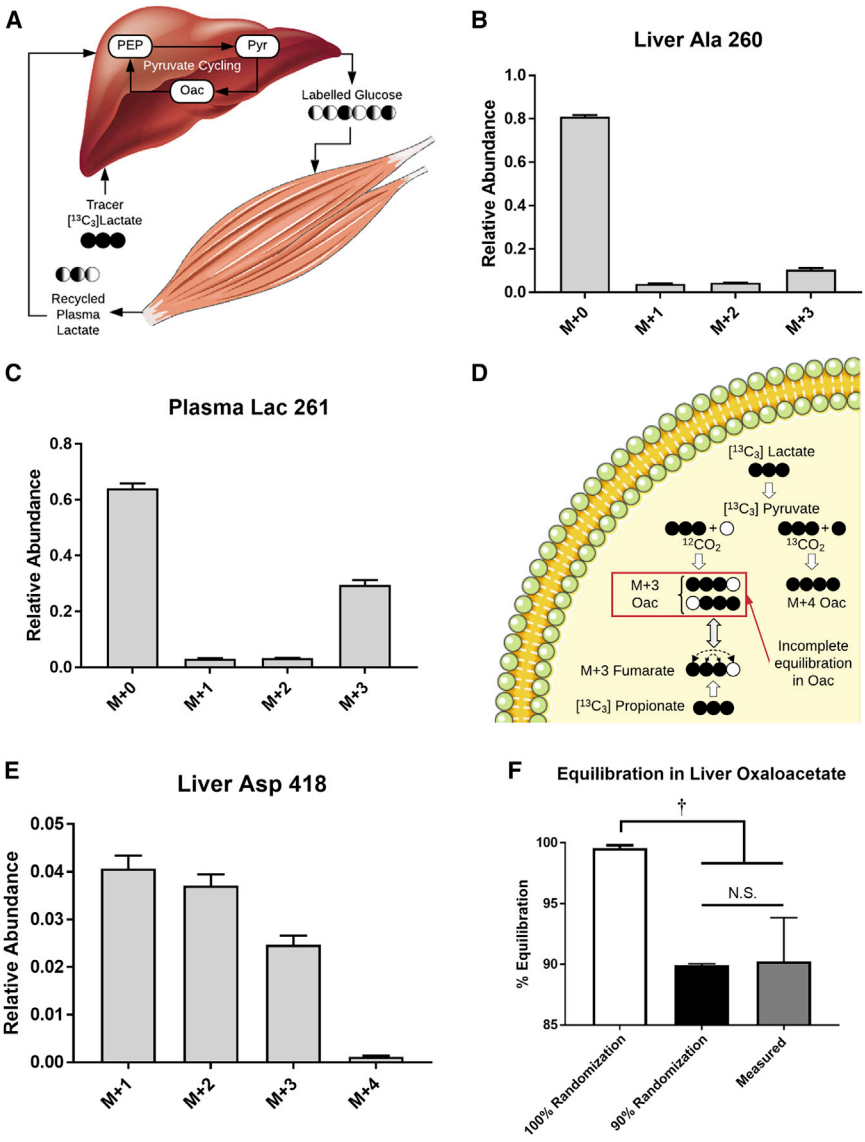

Figure 3. Testing the Assumptions of Secondary Tracer Effects and Fumarate/Oxaloacetate Equilibration in a $^{13}C_3$Lac Infusion Study

(A) Hepatic production of labeled glucose from $^{13}C_3$Lac can be metabolized by the muscle to produce recycled lactate that can contribute to secondary tracer effects (Cori cycling).

(B) MID of liver alanine (*m/z* 260) obtained at the end of the $^{13}C_3$Lac infusion. Data are corrected for natural isotope abundance and presented as means ± SEM (n = 7).

(C) MID of plasma lactate (*m/z* 261) obtained at the end of the $^{13}C_3$Lac infusion. Data are corrected for natural isotope abundance and presented as means ± SEM (n = 7).

(D) CAC isotopomers formed directly from $^{13}C_3$Lac or $^{13}C_3$Prop tracers. Carboxylation of M+3 pyruvate with $^{12}CO_2$ produces M+3 oxaloacetate (Oac) labeled at carbon positions 1–3 (i.e., Oac_{1110}). Reversible exchange between Oac and fumarate results in randomization of Oac_{1110} and Oac_{0111} isotopomers because of the rotational symmetry of fumarate. The extent of equilibration between Oac_{1110} and Oac_{0111} depends on the rate of Oac-fumarate interconversion relative to the rate of lactate anaplerosis. In contrast, anaplerotic flux from propionate must traverse the symmetric fumarate pool prior to exiting the CAC. In the presence of $^{13}CO_2$ recycling, carboxylation of M+3 pyruvate with $^{13}CO_2$ produces M+4 Oac.

(E) The M+4 isotopomer is detected in the MID of liver aspartate (*m/z* 418), indicative of $^{13}CO_2$ recycling. Data are corrected for natural isotope abundance and presented as means ± SEM (n = 7).

(F) Equilibration of M+3 Oac isotopomers derived from $^{13}C_3$Lac. Percent equilibration was assessed using the measured MIDs of Asp418 and Asp390 ions as described in STAR Methods. This empirical estimate was compared with theoretical values obtained from model-simulated MIDs predicted under assumptions of 100% or 90% randomization of Oac produced in the PC reaction. Data are presented as means ± SEM (n = 7); †$p \leq 0.05$.

pyruvate flux into the CAC) (Figure S6). Estimates of liver glutamate anaplerosis were particularly sensitive to changing model assumptions about PDH activity because increased glutamate entry effectively offset reductions in $V_{CS.L}$ so that estimates of $V_{MDH.L}$ were unchanged when PDH was active (Figures S4 and S6). Other liver fluxes were not significantly altered by inclusion of PDH in the reaction network. Importantly, the effects of Cori cycling to reduce pyruvate cycle and CAC fluxes were replicated in models with an active PDH complex ($V_{PDH.L}$) (Figure S6). In summary, estimates of liver pyruvate cycling and CAC-associated fluxes were sensitive to changing model assumptions regarding secondary tracer recycling and equilibration in the CAC. On the other hand, glucose-producing fluxes were robust to changes in these same model assumptions.

Finally, we examined whether an alternative approach for assessing liver pyruvate cycling would be similarly affected by assumptions related to secondary tracer recycling. Perry et al. (2016) previously described a method for estimating liver pyruvate cycling that relies on the measured ratio of [2-^{13}C]alanine to [2-^{13}C]malate enrichments following infusion with [3-^{13}C]lactate. We simulated steady-state ^{13}C enrichments at the C2 positions of malate and alanine derived from [3-^{13}C]lactate based on best-fit flux solutions obtained from the one- or two-compartment expanded model. Both models simulated [2-^{13}C]Ala/[2-^{13}C]Mal ratios that varied linearly with the liver V_{PK+ME}/V_{PC} ratio, but the two-compartment model predicted higher isotopomer ratios compared with the liver-only model (Figure 4C). The divergence between the models was most substantial at the lower range of V_{PK+ME}/V_{PC} flux, where the two-compartment model predicted a non-zero [2-^{13}C]Ala/[2-^{13}C]Mal ratio even in the absence of liver pyruvate cycling because of contributions from extrahepatic

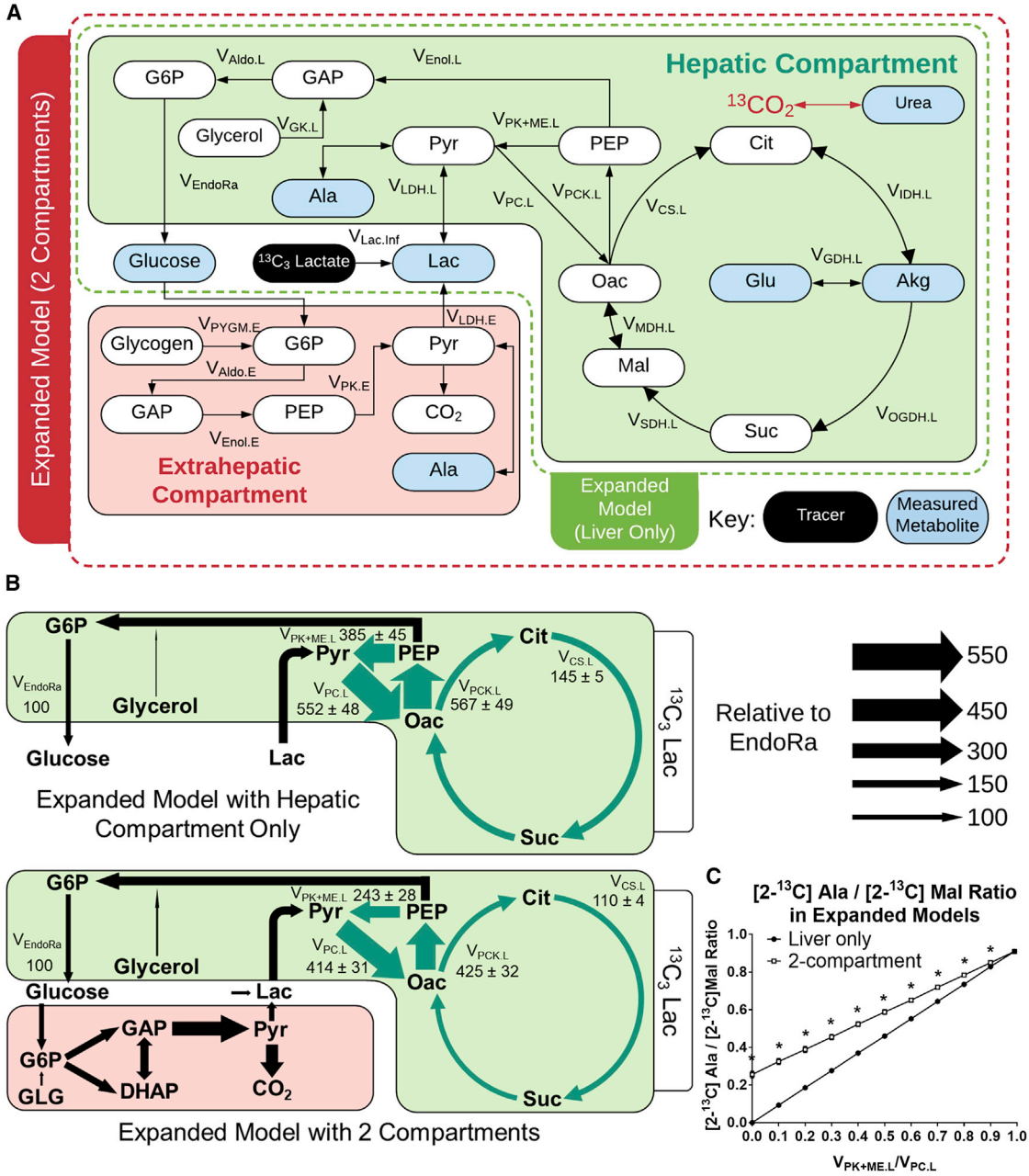

Figure 4. Expansion of the Base Model in Mice Infused with $^{13}C_3$Lac Only

(A) Network diagram showing the expanded model with an extrahepatic compartment to facilitate descriptions of Cori cycling in $^{13}C_3$Lac tracer experiments. A broader set of plasma and tissue measurements was used to constrain the model (Table S3).

(B) Comparison of expanded model flux results with one compartment (liver only) or two compartments, showing relative flux estimates in 19- to 20-h-fasted C57BL/6J mice infused with $^{13}C_3$Lac. Fluxes are normalized to total glucose production (V_{EndoRa} = 100). Fluxes highlighted in green show significant changes between the two models. Data are presented as means ± SEM (n = 7); $p \leq 0.05$.

(C) [2-^{13}C]alanine/[2-^{13}C]malate ratio predicted for varying liver $V_{PK+ME.L}/V_{PC.L}$ ratios in a simulated study using [3-^{13}C]lactate. Simulations were performed using the best-fit solutions obtained from a liver-only or two-compartment expanded model regressed to fit the $^{13}C_3$Lac measurements. Data are presented as means ± SEM (n = 7); *$p \leq 0.01$, determined using unpaired t test without assuming consistent SD.

sources of [2-^{13}C]Ala. This incongruity provides evidence that secondary tracer effects are also embedded in liver flux estimates obtained from other stable isotope approaches because these estimates do not differentiate between pyruvate cycling within the liver or in an extrahepatic compartment.

Expanded Two-Compartment Models Provide Consistent Hepatic Flux Estimates Using $^{13}C_3$Prop/^{2}H and $^{13}C_3$Lac/^{2}H Tracers *In Vivo*

Plasma and liver tissues extracted from mice in prior $^{13}C_3$Prop/^{2}H and $^{13}C_3$Lac/^{2}H studies (assessed with base models in Figure 2D and 2E) were re-analyzed to yield a set of metabolite MIDs similar to those in Figure S3. Expanded models for exchange of $^{13}C/^{12}C$ and $^{2}H/^{1}H$ atoms were constructed to accommodate measurements from $^{13}C_3$Lac/^{2}H and $^{13}C_3$Prop/^{2}H experiments (Figure 5A; Table S4). These models were similar to the expanded ^{13}C-only model in Figure 4A with the following modifications: (1) hydrogen atom transitions were included, (2) reactions to account for infusion of ^{2}H and $^{13}C_3$Prop tracers were added, (3) glycogenolysis was assumed to be active, and (4) glutamate anaplerosis was assumed to be inactive. The latter assumption was necessary because glutamate MID measurements were not attainable from samples collected in $^{13}C_3$Lac/^{2}H and $^{13}C_3$Prop/^{2}H experiments, making the flux from the unenriched anaplerotic source of glutamate ($V_{Glu.source}$) unidentifiable. Hepatic flux estimates obtained from $^{13}C_3$Lac/^{2}H and $^{13}C_3$Prop/^{2}H infusions were similar when regressed with expanded models: V_{EndoRa} and $V_{Enol.L}$ were comparable (Figures 5B and S7), and pyruvate cycle and CAC fluxes were not significantly different (Table S2). Thus, expanded models that allow secondary tracer recycling and data-driven estimation of *in vivo* reaction reversibility provide congruent liver flux estimates with $^{13}C_3$Prop/^{2}H or $^{13}C_3$Lac/^{2}H.

To investigate the effects of model expansion, we compared flux estimates from expanded versus base models using the same tracer datasets. There were no significant differences between fluxes estimated by the expanded and base $^{13}C_3$Prop/^{2}H models. However, the expanded $^{13}C_3$Lac/^{2}H model showed a significant elevation in hepatic pyruvate cycling ($V_{PK+ME.L}$, $V_{PC.L}$, and $V_{PCK.L}$) and CAC ($V_{CS.L}$) fluxes compared with the base $^{13}C_3$Lac/^{2}H model (Table S2). Thus, model expansion had a more pronounced effect on flux estimates obtained from $^{13}C_3$Lac/^{2}H studies than $^{13}C_3$Prop/^{2}H studies.

Finally, we used our expanded model of $^{13}C_3$Prop/^{2}H experiments to assess a ^{13}C NMR approach for estimating liver metabolic fluxes using this same combination of tracers. Jin et al. (2005) previously described a method for estimating liver pyruvate cycling that relies on the measured ratio of (D12−Q)/(D12−D23) multiplets obtained from the C2 resonance of plasma glucose. We adapted our base and expanded models to simulate these multiplet signals (Deja et al., 2020) using best-fit flux solutions obtained from our $^{13}C_3$Prop/^{2}H infusions. Both models simulated C2 multiplet ratios that varied roughly in proportion to liver V_{PK+ME}/V_{PC} flux, with only slight divergence at higher levels of pyruvate cycling flux (Figure 5C). The agreement between the two models can be explained by the approximately offsetting effects of $^{13}CO_2$ recycling and Cori cycling on the simulated C2 multiplet ratio. $^{13}CO_2$ recycling tends to elevate the quartet (Q) signal, whereas Cori cycling tends to decrease it, thus making the (D12−Q)/(D12−D23) ratio insensitive to model expansion. This empirical finding is not a theoretically generalizable result, however, and may depend on the tracer infusion rate, the physiological state of the animals, as well as other methodological parameters.

DISCUSSION

Isotope-based flux analysis is the gold standard for measurements of *in vivo* metabolism and has provided important insights into whole-body fuel utilization, cancer metabolism, insulin resistance, and fatty liver disease (Faubert et al., 2017; Hasenour et al., 2020; Hui et al., 2017; Perry et al., 2015; Satapati et al., 2015; Sunny et al., 2011). Thus, use of MFA to model and interpret data from *in vivo* ILEs is only expected to increase. During an effort to improve the robustness of our own MFA platform for assessing *in vivo* liver metabolism, we noted isotope-specific inconsistencies similar to previous observations that have given rise to a contentious debate in the literature (Befroy et al., 2014, 2015; Satapati et al., 2015). Studies with ^{13}C-propionate administered to humans with fatty liver or high-fat-fed mice have reported dramatic elevations in liver CAC and anaplerotic fluxes compared with controls (Satapati et al., 2012; Sunny et al., 2011). In contrast, studies with ^{13}C-acetate have reported no increases in CAC or anaplerotic fluxes in patients with fatty liver (Petersen et al., 2016). However, the mathematical model used to estimate fluxes in the latter study neglected liver pyruvate kinase (PK) activity and, therefore, did not account for the possibility of liver pyruvate cycling, which is needed to explain the labeling patterns typically observed with ^{13}C NMR analysis of plasma samples obtained from ^{13}C-propionate tracer studies (Burgess et al., 2015).

The omission of PK flux in models of liver metabolism is supported by arguments that "futile" pyruvate cycling is not energetically feasible, that inhibition of PK by glucagon during fasting should prevent pyruvate cycling, and that some experiments with ^{13}C-lactate tracers indicate that liver pyruvate cycling is negligible (Befroy et al., 2015). One explanation for the divergent results of prior studies is that elevated rates of liver anaplerosis and pyruvate cycling reported in some cases may have been an artifact of ^{13}C-propionate administration (Perry et al., 2016). However, large estimates of hepatic PK flux have been reported under fasted conditions across species with radioactive and stable isotopes (Beylot et al., 1995; Jones et al., 1997; Katz et al., 1993; Magnusson et al., 1991). One might expect liver flux analysis in perfusion or *in vitro* to clarify discrepancies in PK flux estimates. However, removal of the liver from the physiological milieu can rapidly alter PK activity (Large et al., 1997; Riou et al., 1985). Liver PK activity is also responsive to endocrine hormone regulation. This has been shown using [3-^{13}C]lactate to assess metabolic fluxes in perfused livers from 48-h-fasted rats in the presence or absence of glucagon (Large et al., 1997). V_{PK} was ~50% the rate of V_{PCK} in control livers, which was reduced to ~20% during perfusion of glucagon (Large et al., 1997). The aforementioned work is one publication among several to yield sizeable estimates for the ratios of V_{PK+ME}/V_{PCK} and V_{PK+ME}/V_{CS} in the liver (Katz et al., 1993; Large and Beylot, 1999; Magnusson et al., 1991); it is noteworthy that no research in these cited publications used isotopic propionate to estimate liver fluxes.

Because of the significance of pyruvate cycling in the interpretation of ILEs and the importance of PK in regulating liver glycolysis and gluconeogenesis, we sought to examine the incongruent findings of prior studies by testing specific modeling assumptions and assessing different combinations of isotope

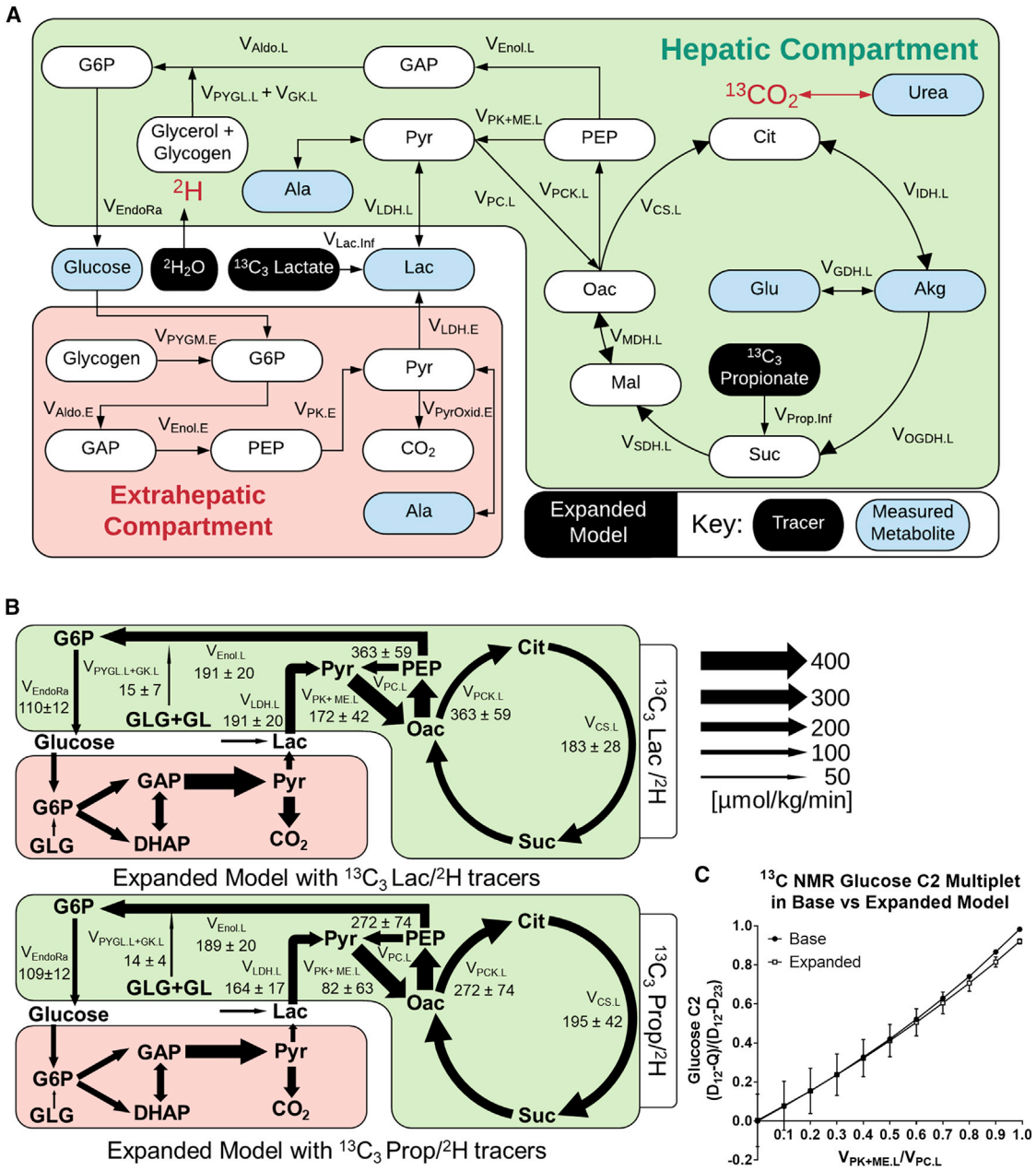

Figure 5. Comparison of $^{13}C_3$Lac/^{2}H and $^{13}C_3$Prop/^{2}H Isotopes for Hepatic Flux Estimation Using Expanded Models of Metabolism

(A) Network map showing the expanded model with $^{13}C_3$Prop/^{2}H or $^{13}C_3$Lac/^{2}H isotopes and highlighting measured metabolites.

(B) Comparison of two-compartment expanded models regressed to $^{13}C_3$Prop/^{2}H or $^{13}C_3$Lac/^{2}H labeling measurements. Absolute flux estimates are shown for 19- to 20-h-fasted C57BL/6J mice. Data are presented as means ± SEM (micromoles per kilogram per minute, n = 5).

(C) Glucose-C2 ^{13}C-NMR (D12−Q)/(D12−D23) multiplet ratio predicted for varying liver $V_{PK+ME.L}/V_{PC.L}$ ratios using different models of the $^{13}C_3$Prop tracer experiment. Simulations were performed using the best-fit solutions obtained from the base model (Figure 2D) or two-compartment expanded model (Figure 5B) regressed to $^{13}C_3$Prop/^{2}H measurements. Data are presented as means ± SEM (n = 4 for the base model, n = 7 for the expanded model).

tracers and measurements that have been used previously to estimate liver metabolic fluxes *in vivo*. We confirmed that assumptions about extrahepatic tracer recycling and equilibration of 4C CAC intermediates can significantly alter estimates of pyruvate cycle fluxes. These assumptions may be sensitive to hormonal and nutritional status and to whether the primary tracer enters "upstream" or "downstream" of Oac. It is noteworthy that multi-compartment models with expanded metabolite labeling measurements and fewer simplifying assumptions still indicated significant liver pyruvate cycling.

Previous work suggests that extrahepatic tissues may not process isotopic propionate and lactate equivalently (Landau et al.,

1993). This has been shown in the perfused heart, where the provision of propionate can influence oxidative metabolism (Purmal et al., 2014). Nevertheless, liver flux estimates using both isotopes achieved reasonable agreement when broader *in vivo* physiology was modeled. Liver V_{PK+ME} flux was reduced but not eliminated by *in vivo* operation of the Cori cycle in models that accounted for extrahepatic metabolism. Total anaplerosis was consistently observed to be higher than the rate of citrate synthase, regardless of the isotope used in the study. Estimates of the V_{PCK}/V_{CS} ratio reported here are within the range observed previously across modeling platforms and species using various isotopes (Befroy et al., 2014; Beylot et al., 1995; Burgess et al., 2005; Jin et al., 2005; Katz et al., 1993; Large and Beylot, 1999; Magnusson et al., 1991; Satapati et al., 2012). These observations perhaps help to resolve some of the recent concerns expressed by others regarding the incompatibility of ^{13}C-labeled propionate or lactate for measurement of hepatic fluxes. Our results also underscore the importance of model design and optimal isotope selection for accuracy and precision of MFA (Metallo et al., 2009).

No differences in plasma glucose concentration, endogenous glucose production, or gluconeogenesis were observed in mice infused with $^{13}C_3$Prop or $^{13}C_3$Lac, consistent with other recently published data (Hasenour et al., 2015; Satapati et al., 2015). The substrate actions of propionate on hepatic metabolism, however, are unclear. Others have reported that propionate increases glucose production and plasma glucose concentrations in rats (Befroy et al., 2014). Conversely, administration of propionate with lactate in perfused liver has been shown to inhibit glucose production (Blair et al., 1973). Similar limitations may also be important for use of $^{13}C_3$Lac because circulating lactate acts as a major carbon shuttle between and within numerous tissues in the body (Hui et al., 2017), and recycled lactate significantly contributes to gluconeogenesis during fasting (Wang et al., 2020). In fact, infusion of [U-$^{13}C_6$]glucose and generation of enriched lactate from extrahepatic tissues may serve as an experimental tracer strategy for estimating endogenous glucose production and gluconeogenesis (Antoniewicz et al., 2006; Cappel et al., 2019). In consideration of these data, we developed expanded models where liver and extrahepatic metabolism were treated as separate compartments bridged by a plasma compartment, and plasma lactate was allowed to equilibrate with extrahepatic pyruvate/alanine.

Affirmative claims regarding the ability of these expanded models to resolve specific peripheral fluxes should be viewed with caution because the extrahepatic compartment was not designed to encompass the gamut of metabolism present outside of the liver. For example, gluconeogenic fluxes from extrahepatic tissues (e.g., kidney) were assumed to have a marginal influence on plasma glucose enrichment. This assumption was validated in part by the acceptable agreement between plasma glucose and liver metabolite enrichments obtained when both were regressed simultaneously using expanded models. It is also plausible that other enriched plasma metabolites not measured here could influence flux solutions. Although the liver displays some functional heterogeneity, liver metabolites were modeled as steady-state components of a single gluconeogenic compartment. This is a limited but reasonable assumption for hepatocytes but not likely to be true for nonparenchymal cells of the liver, which could not be separated from tissue extracts. It is important to also consider that our results are specific to a discrete set of well-controlled *in vivo* conditions; the experimental strategy and results presented here should not necessarily be extrapolated to other designs (e.g., involving significant variations in nutrient load). A carotid artery catheter was surgically implanted to avoid mouse handling during plasma sample collection. It is not known whether other sampling procedures might affect the endocrine state of the mouse and interfere with flux estimates.

Model-based regression approaches are needed to account for the complexities of *in vivo* stable isotope experiments and to rigorously test assumptions used in the calculation of metabolic fluxes. The availability of flexible modeling tools (e.g., INCA [Young, 2014], Metran [Yoo et al., 2008], and 13CFLUX2 [Weitzel et al., 2013]) now make this increasingly possible. Comprehensive isotopomer modeling and integrative flux analysis methodologies have the potential to reconcile apparently divergent results and identify flux estimates that are sensitive to methodological differences or, conversely, robust to a variety of study designs and assumptions. The INCA software is generalizable to tracers with any combination of labeled atoms, and we can readily construct models that take differences in tracers or administration routes into account. Furthermore, INCA can model transient labeling experiments that result from a step input of labeled tracer (Young, 2014). As a result, we expect that the findings of the current study are applicable to a wide range of experimental systems used in metabolism research, and the models can be adapted to other possible study designs.

Here we demonstrate the significance of secondary tracer effects and incomplete isotope equilibration on flux estimates obtained from *in vivo* ILEs, which can affect a variety of flux modeling approaches. When we expanded our base model by adding several liver-specific metabolite measurements while relaxing assumptions related to isotopic equilibrium and tracer recycling, our results indicated that significant liver pyruvate cycling persisted under fasting conditions. Furthermore, we did not find evidence that exogenous propionate administration had a significant effect on glucose-producing or pyruvate cycling fluxes. Although estimates of liver pyruvate cycling were influenced by Cori cycle activity, accounting for extrahepatic metabolism in an expanded multi-compartment MFA model did not abolish liver pyruvate cycle flux. One potential way to further examine the role and importance of pyruvate cycling in the liver would be to utilize liver-specific, genetic, or pharmacological inhibition of the PK enzyme.

STAR★METHODS

Detailed methods are provided in the online version of this paper and include the following:

- KEY RESOURCES TABLE
- RESOURCE AVAILABILITY
  - Lead Contact
  - Materials Availability
  - Data and Code Availability

SUPPLEMENTAL INFORMATION

Supplemental Information can be found online at https://doi.org/10.1016/j.celrep.2020.107986.

ACKNOWLEDGMENTS

We thank Vanderbilt's Mouse Metabolic Phenotyping Center (MMPC) for assistance with some *in vivo* studies described here. This research was supported by NIH grants R01 DK106348 and U01 CA235508, the Integrated Training in Engineering and Diabetes NIH training grant (T32 DK101003), and the Vanderbilt MMPC (NIH grant U24 DK059637).

AUTHOR CONTRIBUTIONS

C.M.H. designed and performed experiments, analyzed data, constructed models, and wrote the manuscript. M.R. analyzed data, constructed models, and co-wrote the manuscript. J.D.Y. supervised the project, constructed models, and co-wrote the manuscript.

DECLARATION OF INTERESTS

J.D.Y. is a co-founder, shareholder, and company director of Metalytics. C.M.H. is an employee of Metalytics.

Received: November 20, 2018
Revised: June 1, 2020
Accepted: July 13, 2020
Published: August 4, 2020

REFERENCES

Antoniewicz, M.R., Kelleher, J.K., and Stephanopoulos, G. (2006). Determination of confidence intervals of metabolic fluxes estimated from stable isotope measurements. Metab. Eng. *8*, 324–337.

Antoniewicz, M.R., Kelleher, J.K., and Stephanopoulos, G. (2011). Measuring deuterium enrichment of glucose hydrogen atoms by gas chromatography/mass spectrometry. Anal. Chem. *83*, 3211–3216.

Ayala, J.E., Bracy, D.P., McGuinness, O.P., and Wasserman, D.H. (2006). Considerations in the design of hyperinsulinemic-euglycemic clamps in the conscious mouse. Diabetes *55*, 390–397.

Befroy, D.E., Perry, R.J., Jain, N., Dufour, S., Cline, G.W., Trimmer, J.K., Brosnan, J., Rothman, D.L., Petersen, K.F., and Shulman, G.I. (2014). Direct assessment of hepatic mitochondrial oxidative and anaplerotic fluxes in humans using dynamic 13C magnetic resonance spectroscopy. Nat. Med. *20*, 98–102.

Befroy, D.E., Kibbey, R.G., Perry, R.J., Petersen, K.F., Rothman, D.L., and Shulman, G.I. (2015). Response to burgess. Nat. Med. *21*, 109–110.

Beylot, M., Soloviev, M.V., David, F., Landau, B.R., and Brunengraber, H. (1995). Tracing hepatic gluconeogenesis relative to citric acid cycle activity in vitro and in vivo. Comparisons in the use of [3-13C]lactate, [2-13C]acetate, and α-keto[3-13C]isocaproate. J. Biol. Chem. *270*, 1509–1514.

Blair, J.B., Cook, D.E., and Lardy, H.A. (1973). Interaction of propionate and lactate in the perfused rat liver. Effects of glucagon and oleate. J. Biol. Chem. *248*, 3608–3614.

Burgess, S.C., Jeffrey, F.M.H., Storey, C., Milde, A., Hausler, N., Merritt, M.E., Mulder, H., Holm, C., Sherry, A.D., and Malloy, C.R. (2005). Effect of murine strain on metabolic pathways of glucose production after brief or prolonged fasting. Am. J. Physiol. Endocrinol. Metab. *289*, E53–E61.

Burgess, S.C., Merritt, M.E., Jones, J.G., Browning, J.D., Sherry, A.D., and Malloy, C.R. (2015). Limitations of detection of anaplerosis and pyruvate cycling from metabolism of [1-(13)C] acetate. Nat. Med. *21*, 108–109.

Cappel, D.A., Deja, S., Duarte, J.A.G., Kucejova, B., Iñigo, M., Fletcher, J.A., Fu, X., Berglund, E.D., Liu, T., Elmquist, J.K., et al. (2019). Pyruvate-Carboxylase-Mediated Anaplerosis Promotes Antioxidant Capacity by Sustaining TCA Cycle and Redox Metabolism in Liver. Cell Metab. *29*, 1291–1305.e8.

Deja, S., Fu, X., Fletcher, J.A., Kucejova, B., Browning, J.D., Young, J.D., and Burgess, S.C. (2020). Simultaneous tracers and a unified model of positional and mass isotopomers for quantification of metabolic flux in liver. Metab. Eng. *59*, 1–14.

Faubert, B., Li, K.Y., Cai, L., Hensley, C.T., Kim, J., Zacharias, L.G., Yang, C., Do, Q.N., Doucette, S., Burguete, D., et al. (2017). Lactate Metabolism in Human Lung Tumors. Cell *171*, 358–371.e9.

Hasenour, C.M., Wall, M.L., Ridley, D.E., Hughey, C.C., James, F.D., Wasserman, D.H., and Young, J.D. (2015). Mass spectrometry-based microassay of (2)H and (13)C plasma glucose labeling to quantify liver metabolic fluxes in vivo. Am. J. Physiol. Endocrinol. Metab. *309*, E191–E203.

Hasenour, C.M., Kennedy, A.J., Bednarski, T., Trenary, I.A., Eudy, B.J., da Silva, R.P., Boyd, K.L., and Young, J.D. (2020). Vitamin E does not prevent Western diet-induced NASH progression and increases metabolic flux dysregulation in mice. J. Lipid Res. *61*, 707–721.

Hui, S., Ghergurovich, J.M., Morscher, R.J., Jang, C., Teng, X., Lu, W., Esparza, L.A., Reya, T., Le Zhan, L., Yanxiang Guo, J., et al. (2017). Glucose feeds the TCA cycle via circulating lactate. Nature *551*, 115–118.

Jin, E.S., Burgess, S.C., Merritt, M.E., Sherry, A.D., and Malloy, C.R. (2005). Differing mechanisms of hepatic glucose overproduction in triiodothyronine-treated rats vs. Zucker diabetic fatty rats by NMR analysis of plasma glucose. Am. J. Physiol. Endocrinol. Metab. *288*, E654–E662.

Jones, J.G., Naidoo, R., Sherry, A.D., Jeffrey, F.M.H., Cottam, G.L., and Malloy, C.R. (1997). Measurement of gluconeogenesis and pyruvate recycling in the rat liver: a simple analysis of glucose and glutamate isotopomers during metabolism of [1,2,3-(13)C3]propionate. FEBS Lett. *412*, 131–137.

Katz, J., Wals, P., and Lee, W.-N.P. (1993). Isotopomer studies of gluconeogenesis and the Krebs cycle with 13C-labeled lactate. J. Biol. Chem. *268*, 25509–25521.

Landau, B.R. (1991). Correction of tricarboxylic acid cycle exchange in gluconeogenesis: why the y's are wrong. Am. J. Physiol. *261*, E673–E676.

Landau, B.R., Schumann, W.C., Chandramouli, V., Magnusson, I., Kumaran, K., and Wahren, J. (1993). 14C-labeled propionate metabolism in vivo and estimates of hepatic gluconeogenesis relative to Krebs cycle flux. Am. J. Physiol. *265*, E636–E647.

Large, V., and Beylot, M. (1999). Modifications of citric acid cycle activity and gluconeogenesis in streptozotocin-induced diabetes and effects of metformin. Diabetes *48*, 1251–1257.

Large, V., Brunengraber, H., Odeon, M., and Beylot, M. (1997). Use of labeling pattern of liver glutamate to calculate rates of citric acid cycle and gluconeogenesis. Am. J. Physiol. *272*, E51–E58.

Magnusson, I., Schumann, W.C., Bartsch, G.E., Chandramouli, V., Kumaran, K., Wahren, J., and Landau, B.R. (1991). Noninvasive tracing of Krebs cycle metabolism in liver. J. Biol. Chem. *266*, 6975–6984.

Metallo, C.M., Walther, J.L., and Stephanopoulos, G. (2009). Evaluation of 13C isotopic tracers for metabolic flux analysis in mammalian cells. J. Biotechnol. *144*, 167–174.

Perry, R.J., Camporez, J.G., Kursawe, R., Titchenell, P.M., Zhang, D., Perry, C.J., Jurczak, M.J., Abudukadier, A., Han, M.S., Zhang, X.M., et al. (2015).

Hepatic acetyl CoA links adipose tissue inflammation to hepatic insulin resistance and type 2 diabetes. Cell *160*, 745–758.

Perry, R.J., Borders, C.B., Cline, G.W., Zhang, X.M., Alves, T.C., Petersen, K.F., Rothman, D.L., Kibbey, R.G., and Shulman, G.I. (2016). Propionate increases hepatic pyruvate cycling and anaplerosis and alters mitochondrial metabolism. J. Biol. Chem. *291*, 12161–12170.

Petersen, K.F., Befroy, D.E., Dufour, S., Rothman, D.L., and Shulman, G.I. (2016). Assessment of Hepatic Mitochondrial Oxidation and Pyruvate Cycling in NAFLD by (13)C Magnetic Resonance Spectroscopy. Cell Metab. *24*, 167–171.

Purmal, C., Kucejova, B., Sherry, A.D., Burgess, S.C., Malloy, C.R., and Merritt, M.E. (2014). Propionate stimulates pyruvate oxidation in the presence of acetate. Am. J. Physiol. Heart Circ. Physiol. *307*, H1134–H1141.

Riou, J.P., Audigier, C., Laville, M., Beylot, M., Pigeon, P., and Mornex, R. (1985). Dephosphorylation of L-pyruvate kinase during rat liver hepatocyte isolation. Arch. Biochem. Biophys. *236*, 321–327.

Satapati, S., Sunny, N.E., Kucejova, B., Fu, X., He, T.T., Méndez-Lucas, A., Shelton, J.M., Perales, J.C., Browning, J.D., and Burgess, S.C. (2012). Elevated TCA cycle function in the pathology of diet-induced hepatic insulin resistance and fatty liver. J. Lipid Res. *53*, 1080–1092.

Satapati, S., Kucejova, B., Duarte, J.A.G., Fletcher, J.A., Reynolds, L., Sunny, N.E., He, T., Nair, L.A., Livingston, K.A., Fu, X., et al. (2015). Mitochondrial metabolism mediates oxidative stress and inflammation in fatty liver. J. Clin. Invest. *125*, 4447–4462.

Schumann, W.C., Magnusson, I., Chandramouli, V., Kumaran, K., Wahren, J., and Landau, B.R. (1991). Metabolism of [2-14C]acetate and its use in assessing hepatic Krebs cycle activity and gluconeogenesis. J. Biol. Chem. *266*, 6985–6990.

Sunny, N.E., Parks, E.J., Browning, J.D., and Burgess, S.C. (2011). Excessive hepatic mitochondrial TCA cycle and gluconeogenesis in humans with nonalcoholic fatty liver disease. Cell Metab. *14*, 804–810.

Wang, Y., Kwon, H., Su, X., and Wondisford, F.E. (2020). Glycerol not lactate is the major net carbon source for gluconeogenesis in mice during both short and prolonged fasting. Mol. Metab. *31*, 36–44.

Weitzel, M., Nöh, K., Dalman, T., Niedenführ, S., Stute, B., and Wiechert, W. (2013). 13CFLUX2–high-performance software suite for (13)C-metabolic flux analysis. Bioinformatics *29*, 143–145.

Yoo, H., Antoniewicz, M.R., Stephanopoulos, G., and Kelleher, J.K. (2008). Quantifying reductive carboxylation flux of glutamine to lipid in a brown adipocyte cell line. J. Biol. Chem. *283*, 20621–20627.

Young, J.D. (2014). INCA: a computational platform for isotopically non-stationary metabolic flux analysis. Bioinformatics *30*, 1333–1335.

STAR★METHODS

KEY RESOURCES TABLE

REAGENT or RESOURCE	SOURCE	IDENTIFIER
Chemicals, Peptides, and Recombinant Proteins		
Methoxamine (MOX) Reagent	Thermo Fisher Scientific	Cat#TS-45950
MTBSTFA + 1% TBDMCS Silylation Reagent	Thermo Fisher Scientific	Cat#TS-48927
Sodium Propionate ($^{13}C_3$, 99%)	Cambridge Isotope Laboratories	Cat#CLM-1865-PK
Sodium L-Lactate ($^{13}C_3$, 98%) 20% W/W in H_2O	Cambridge Isotope Laboratories	Cat#CLM-1579-MPT-PK
D-Glucose (6,6,-D_2, 99%)	Cambridge Isotope Laboratories	Cat#DLM-349-1
Deuterium Oxide (D, 99.9%)	Cambridge Isotope Laboratories	Cat#DLM-4-100
Deposited Data		
MID enrichment data	This paper; Mendeley Data	https://dx.doi.org/10.17632/c3kvmfsmdk.2
Experimental Models: Organisms/Strains		
Mouse: C57BL/6J	The Jackson Laboratory	https://www.jax.org/strain/000664; RRID: IMSR_JAX:000664
Software and Algorithms		
Prism 7	GraphPad	https://www.graphpad.com
MATLAB 9.1	Mathworks	https://www.mathworks.com
Microsoft Excel 2015	Microsoft	https://www.microsoft.com/en-us/
INCA (Isotopomer Network Compartmental Analysis)	Young (2014)	https://academic.oup.com/bioinformatics/article-lookup/doi/10.1093/bioinformatics/btu015

RESOURCE AVAILABILITY

Lead Contact

Further information and requests for resources and reagents should be directed to and will be fulfilled by the Lead Contact, Jamey Young (j.d.young@vanderbilt.edu).

Materials Availability

This study did not generate new unique reagents.

Data and Code Availability

The dataset supporting each metabolic flux model has been uploaded to Mendeley Data and is accessible at https://dx.doi.org/10.17632/c3kvmfsmdk.2

EXPERIMENTAL MODEL AND SUBJECT DETAILS

All animal experiments were performed in accordance with institutional guidelines and approved protocol at Vanderbilt University Animal Care and Use Committee. C57BL/6J mice were purchased from Jackson Laboratories (Bar Harbor, ME) and studied at ~10-11wks of age. Male mice were studied to limit any potential variation caused by estrus cycles and for a closer base of comparison to previous studies. Mice were provided free access to a standard chow diet (LabDiet 5001, PMI Nutrition International) and water and maintained on a 12:12h light-dark cycle in a temperature (23°C) and humidity stable environment.

METHOD DETAILS

In vivo Procedures in the Mouse

Indwelling catheters were surgically implanted in the jugular vein and carotid artery ~1wk prior to experimentation for infusing and sampling, respectively, as previously described (Ayala et al., 2006). *In vivo* studies were performed identically to those described in detail elsewhere in long-term (~19-20hr) fasted mice (Hasenour et al., 2015). Briefly, mice received an intravenous primed, continuous infusion of [6,6-$^2H_2$]glucose (440μmol/kg + 4.4μmol/kg/min), bolus of ^2H_2O to enrich body water to 4.5% (abbreviated

collectively as ^{2}H), and a primed, continuous infusion of $^{13}C_3$Prop (1.1mmol/kg + 0.055mmol/kg/min) or $^{13}C_3$Lac (0.160mmol/kg + 0.040mmol/kg/min) (Cambridge Isotope Laboratories, Tewksbury MA). Isotopes were delivered over a 4hr time course, as previously described. A separate cohort of overnight fasted mice was infused with a primed, continuous infusion of $^{13}C_3$Lac (0.160mmol/kg + 0.040mmol/kg/min, respectively) for 120min in the absence of ^{2}H isotopes for relative liver flux estimation. Mice were sacrificed through cervical dislocation and liver tissue was rapidly excised and freeze-clamped in liquid nitrogen at the close of the study; plasma samples and tissues obtained at the end of the study were stored at −80°C prior to analysis.

Metabolite Extraction, Derivatization, and GC-MS

Plasma glucose was extracted and derivatized according to protocols developed elsewhere (Antoniewicz et al., 2011). Following acetone or a biphasic methanol/water/chloroform extraction, polar plasma (~10-50μL) and liver (~30-50mg) metabolites were converted to their methoxamine *tert*-butylsylil derivatives (TBDMS) using MBTSTFA+1% TBDMCS (ThermoFisher Scientific, Waltham MA). Glucose and other metabolite derivatives were injected in an Agilent 7890A gas chromatograph equipped with an HP-5ms capillary column and 5975C mass spectrometer in scan mode for analysis of isotopic enrichment. Metabolites were identified through comparison to a library of known standards, and the accuracy of MID measurements was validated through an assessment of unenriched control samples. Post hoc simulations for metabolite MIDs were performed following best-fit flux regression for each mouse.

Metabolic Flux Analysis (MFA)

All metabolic models were constructed using the Isotopomer Network Compartmental Analysis (INCA) software package (accessible at http://mfa.vueinnovations.com/mfa; Young, 2014); metabolic networks and carbon/hydrogen atom transitions for each modeled reaction are summarized in Tables S1, S3, and S4. Flux models were constructed from classical biochemical reactions with consideration to those published previously (Antoniewicz et al., 2006; Jones et al., 1997; Magnusson et al., 1991). Unless otherwise noted, assumptions used for flux analysis were the same as those provided in a previous publication (Hasenour et al., 2015). MIDs for glucose, plasma and liver polar metabolites were introduced into INCA for flux regression. After constraining citrate synthase flux ($V_{CS.L}$) to an arbitrary value of 100, relative fluxes were estimated by minimizing the sum of squared residuals (SSRs) between simulated and experimentally derived MIDs. Measurement uncertainties were estimated based on the root-mean square error of unenriched control samples and/or the standard error of measurement of technical GC-MS replicates. Best-fit flux estimates were obtained from least-squares regression starting from at least 25 random initial values. Goodness of fit was assessed by a chi-square test, and 95% flux confidence intervals were calculated by evaluating the sensitivity of SSRs to variations in flux values (Antoniewicz et al., 2006). In studies where both $^{13}C/^{2}H$ isotopes were infused, relative fluxes were converted to absolute fluxes using the known [6,6-$^{2}H_2$]glucose infusion rate and mouse weights. For mice infused with $^{13}C/^{2}H$ isotopes, glucose-producing flux from glycerol ($V_{GK.L}$) was summed with glycogen ($V_{PYGL.L}$) and presented in hexose units ($V_{PYGL+GK.L}$).

MIDs and NMR positional enrichments were simulated in INCA using the best-fit flux solutions obtained from *in vivo* labeling experiments. Where appropriate, urea and lactate enrichments obtained during the isotopic steady state were included in the liver flux regressions. An increase in the ^{13}C enrichment of the CO_2 pool *in vivo* is anticipated to some extent, given the introduction of propionate or lactate isotopes into the CAC. A modeling approach was taken to accommodate the reintroduction of locally synthesized $^{13}CO_2$ in the liver in a previous publication (Hasenour et al., 2015). Here, $^{13}CO_2$/bicarbonate enrichment was assumed to equilibrate with the carbonyl carbon of urea (retained by the urea-TBMDS *m/z* 231 ion), since carbamoyl phosphate is formed from HCO_3^- in hepatic mitochondria. As such, the Urea231 enrichment was used as a proxy for $^{13}CO_2$, similar to that applied elsewhere (Magnusson et al., 1991). The MIDs of additional metabolites (e.g., Lac261 ion as a measure of lactate enrichment) were included in specific flux regressions as described in Results (Table S5). Unless otherwise noted, a two-tailed t test was used to test for differences with significance at $p \leq 0.05$.

MFA Model Terminology

$^{13}C_3$Lac	[$^{13}C_3$]Lactate
$^{13}C_3$Prop	Sodium [$^{13}C_3$]Propionate
AcCoA	Acetyl-CoA
Akg	α-Ketoglutarate
Ala	Alanine
BPG	1,3-Bisphosphoglycerate
CAC	Citric acid cycle
Cit	Citrate
CO_2	Carbon dioxide

(*Continued on next page*)

Continued	
DHAP	Dihydroxyacetone Phosphate
FH	Fumarate hydratase
Fum	Fumarate
G6P	Glucose-6-phosphate
GAP	Glyceraldehyde-3-phosphate
GL	Glycerol
GLG	Glycogen
Glu	Glutamate
Glu.source	Unenriched anaplerotic source of glutamate
H6P	Hexose-6-phosphate
ILE	Isotope labeling experiments
Lac	Lactate
Lac.source	Unenriched anaplerotic source lactate
Mal	Malate
MID	mass isotopomer distribution
NMR	Nuclear magnetic resonance
Oac	Oxaloacetate
PEP	Phosphoenolpyruvate
PropCoA	Propionyl-CoA
Pyr	Pyruvate
Suc	Succinate
SucCoA	Succinyl-CoA
T3P	Triose-3-phosphate
TPI	Triose phosphate isomerase
V_{ALT}	Flux between Pyr and Ala
V_{Aldo}	Flux between H6P and T3P or F1,6BP, GAP, and DHAP
V_{CS}	Flux from Oac and AcCoA to Cit
V_{EndoRa}	Endogenous glucose production
V_{Enol}	Flux from PEP to BPG
V_{FH}	Flux between Mal and Fum
V_{GAPDH}	Flux between T3P or GAP and PEP
V_{GDH}	Flux between Glu and αKG
V_{GK}	Flux from glycerol to T3P or DHAP
$V_{Glu.source}$	Flux from unenriched anaplerotic source of glutamate
V_{GPI}	Glucose Phosphate Isomerase
$V_{Glc.inf}$	[6,6-$^{2}H_{2}$]glucose infusion
V_{HK}	Flux from Glc to G6P
V_{IDH}	Flux circuit between Cit and αKG
$V_{Lac.inf}$	[$^{13}C_{3}$]lactate infusion
$V_{Lac.source}$	Flux from unenriched anaplerotic source of lactate
$V_{LacTransport}$	Lac transport from the plasma into the liver
V_{LDH}	Flux from Lactate to Pyruvate
V_{MDH}	Flux between Oac and Mal
V_{OGDH}	Flux from αKG to SucCoA
V_{PC}	Flux from Pyr to Oac
V_{PCC}	Flux from PropCoA to SucCoA
V_{PCK}	Flux from Oac to PEP
V_{PDH}	Flux from Pyr to AcCoA

(*Continued on next page*)

Continued	
V_{PK+ME}	Contribution of pyruvate kinase (PK) and malic enzyme (ME) to Pyr
$V_{Prop.inf}$	[$^{13}C_3$]propionate infusion
V_{PYGL}	Flux from glycogen to G6P in liver
$V_{PYGL+GK}$	Combined flux from glycogen (VPYGL) and glycerol (0.5VGK) to endogenous glucose production in hexose units
V_{PYGM}	Flux from glycogen to G6P in muscle
$V_{PyrOxid}$	Metabolism of Pyr to CO_2
V_{SCS}	Flux from SucCoA to Suc
V_{SDH}	Flux from Suc to Fum
V_{TPI}	Flux between DHAP and GAP
V_{Tracer}	$^{13}C_3$Lac or $^{13}C_3$Prop tracer flux into the liver

Correction of Liver Oxaloacetate Isotopomers to Account for $^{13}CO_2$ Recycling

In the absence of $^{13}CO_2$ recycling, the fully labeled M+4 isotopomer Oac_{1111} should exhibit negligible abundance and only the M+3 oxaloacetate isotopomers Oac_{1110} and Oac_{0111} should be formed from $^{13}C_3$Lac infusion. Yet, after correcting the aspartate MID for natural isotopic background, significant M+4 enrichment was detected (Figure 3E), which stems from carboxylation of M+3 pyruvate with recycled $^{13}CO_2$ (Figure 3D). Because $^{13}CO_2$ can lead to production of M+3 oxaloacetate isotopomers other than Oac_{1110} and Oac_{0111}, the measured MIDs of alanine (a proxy for liver pyruvate) and urea (a proxy for liver CO_2) were used to mathematically correct the M+3 oxaloacetate isotopomers to account for contributions from $^{13}CO_2$ recycling:

$$Oac^{cor}_{1234}(M+3) = Oac_{1234}(M+3) + \frac{V_{PC}}{V_{\Sigma Ana}} \cdot {}^{13}CO_2 \cdot [Pyr_{123}(M+3) - Pyr_{123}(M+2)]$$

$$Oac^{cor}_{234}(M+3) = Oac_{234}(M+3) - \frac{V_{PC}}{V_{\Sigma Ana}} \cdot {}^{13}CO_2 \cdot Pyr_{23}(M+2),$$

where

$\boldsymbol{Oac_{1234}(M+3)}$ = M+3 abundance of Asp418 fragment ion (derived from carbons 1-4 of oxaloacetate)
$\boldsymbol{Oac_{234}(M+3)}$ = M+3 abundance of Asp390 fragment ion (derived from carbons 2-4 of oxaloacetate)
$\boldsymbol{Oac^{cor}_{1234}(M+3)}$ = M+3 abundance of Asp418 after correction for $^{13}CO_2$ recycling
$\boldsymbol{Oac^{cor}_{234}(M+3)}$ = M+3 abundance of Asp390 after correction for $^{13}CO_2$ recycling
$\boldsymbol{Pyr_{123}(M+3)}$ = M+3 abundance of Ala260 fragment ion (derived from carbons 1-3 of pyruvate)
$\boldsymbol{Pyr_{123}(M+2)}$ = M+2 abundance of Ala260
$\boldsymbol{Pyr_{23}(M+2)}$ = M+2 abundance of Ala232 fragment ion (derived from carbons 2-3 of pyruvate)
$\boldsymbol{^{13}CO_2}$ = M+1 abundance of Urea231 fragment ion (derived from liver CO_2),

and the ratio of pyruvate carboxylase flux (V_{PC}) to total anaplerosis ($V_{\sum Ana}$) is determined by:

$$\frac{V_{PC}}{V_{\Sigma Ana}} = \frac{Oac_{1234}(M+4)}{Pyr_{123}(M+3) \cdot {}^{13}CO_2}.$$

All MIDs were corrected for natural stable isotope abundance prior to applying the above equations.

Calculation of Percent Equilibration in the 4C reactions of the CAC

If oxaloacetate fully equilibrates with rotationally symmetric CAC intermediates (i.e., fumarate and succinate) through reversible exchange, an equal abundance of the M+3 oxaloacetate isotopomers Oac_{1110} and Oac_{0111} would be expected (Figure 3D). However, incomplete equilibration would cause the abundance of Oac_{1110} (formed directly from pyruvate carboxylation) to exceed the abundance of Oac_{0111} (formed from reversible exchange with fumarate). Once the corrected oxaloacetate M+3 abundances were calculated as described above, the abundances of Oac_{1110} and Oac_{0111} positional isotopomers formed from $^{13}C_3$Lac were determined as follows:

$$Oac_{0111} = Oac^{cor}_{234}(M+3)$$

$$Oac_{1110} = Oac^{cor}_{1234}(M+3) - Oac^{cor}_{234}(M+3).$$

These abundances were then used to assess the percentage isotope equilibration using the equation:

$$\%Equilibration = \left(1 - \frac{Oac_{1110} - Oac_{0111}}{Oac_{1110} + Oac_{0111}}\right) \times 100\%$$

QUANTIFICATION AND STATISTICAL ANALYSIS

All data were analyzed using an unpaired Student's t test without assuming a consistent standard deviation between groups. Biological replicates and significance values for each analysis are noted in each figure caption.

Cell Reports, Volume *32*

Supplemental Information

In Vivo Estimates of Liver Metabolic Flux Assessed by ^{13}C-Propionate and ^{13}C-Lactate Are Impacted by Tracer Recycling and Equilibrium Assumptions

Clinton M. Hasenour, Mohsin Rahim, and Jamey D. Young

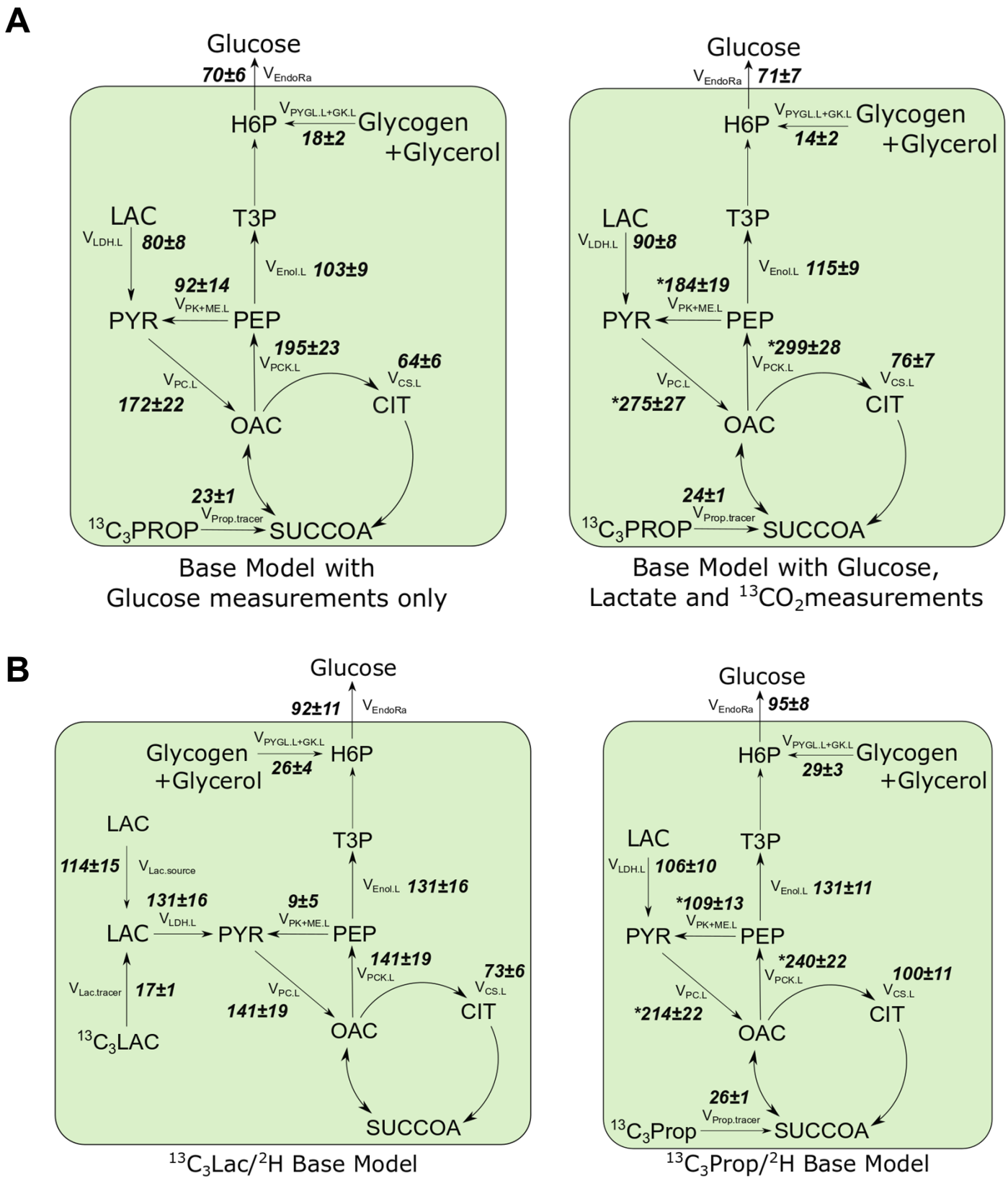

Figure S1. Regression of base model to specific measurement sets. Related to Figures 2, S2, and Table S1

(A) Flux estimates obtained from the base model using plasma glucose MIDs alone contrasted with those that included $^{13}CO_2$ and plasma lactate measurements in the flux regression. Data are presented as means (μmol/kg/min) ± SEM, (n=4) *p<0.05 vs. base model with glucose measurements only

(B) Base model flux estimates from mice infused with $^{13}C_3$Lac/^{2}H or $^{13}C_3$Prop/^{2}H isotopes. Data are presented as means (μmol/kg/min) ± SEM (n=6-7) *p<0.05 vs. $^{13}C_3$Lac/^{2}H base model

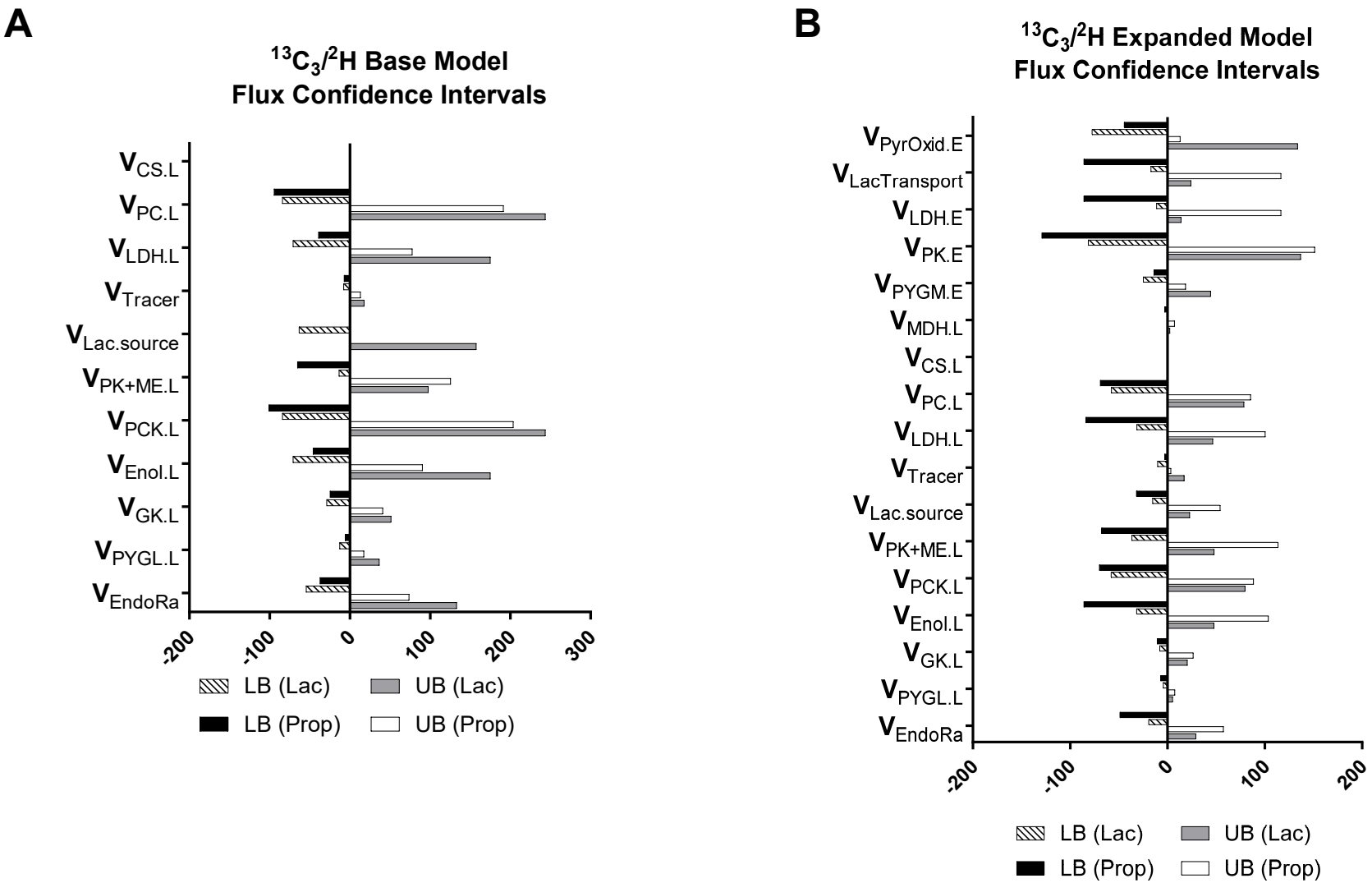

Figure S2. Confidence interval widths in dual tracer models. Related to Figures 2 and 5

95% confidence intervals were calculated for relative hepatic and extrahepatic fluxes in INCA.

(A) $^{13}C_3$Lac/^{2}H (SSR Ave: 19.9±3.5, Expected Range: 11-36.8 DOF: 22) and $^{13}C_3$Prop/^{2}H Base Models (SSR Ave: 32.5±5.4, Expected Range: 11-36.8 DOF: 22). V_{Tracer} represents the flux $V_{Lac.tracer}$ or $V_{Prop.tracer}$ in the liver compartment, depending on the experiment

(B) $^{13}C_3$Lac/^{2}H (SSR Ave: 78.4±8.3, Expected Range: 49.6-96.2, DOF: 72) and $^{13}C_3$Prop/^{2}H Expanded Models (SSR Ave: 70.9±8.1, Expected Range: 49.6-96.2, DOF: 72). V_{Tracer} represents the flux $V_{Lac.inf}$ in blood plasma or the flux of $V_{Prop.inf}$ in the liver compartment, depending on the experiment

Upper and lower bounds are presented as the mean differences (x-axis) from the relative flux estimates (n=5-7). Ranges are expressed relative to $V_{CS.L}$=100. The Expected Range of the SSR is calculated from the 95% confidence limits of a chi-square cumulative distribution function with the indicated degrees of freedom (DOF)

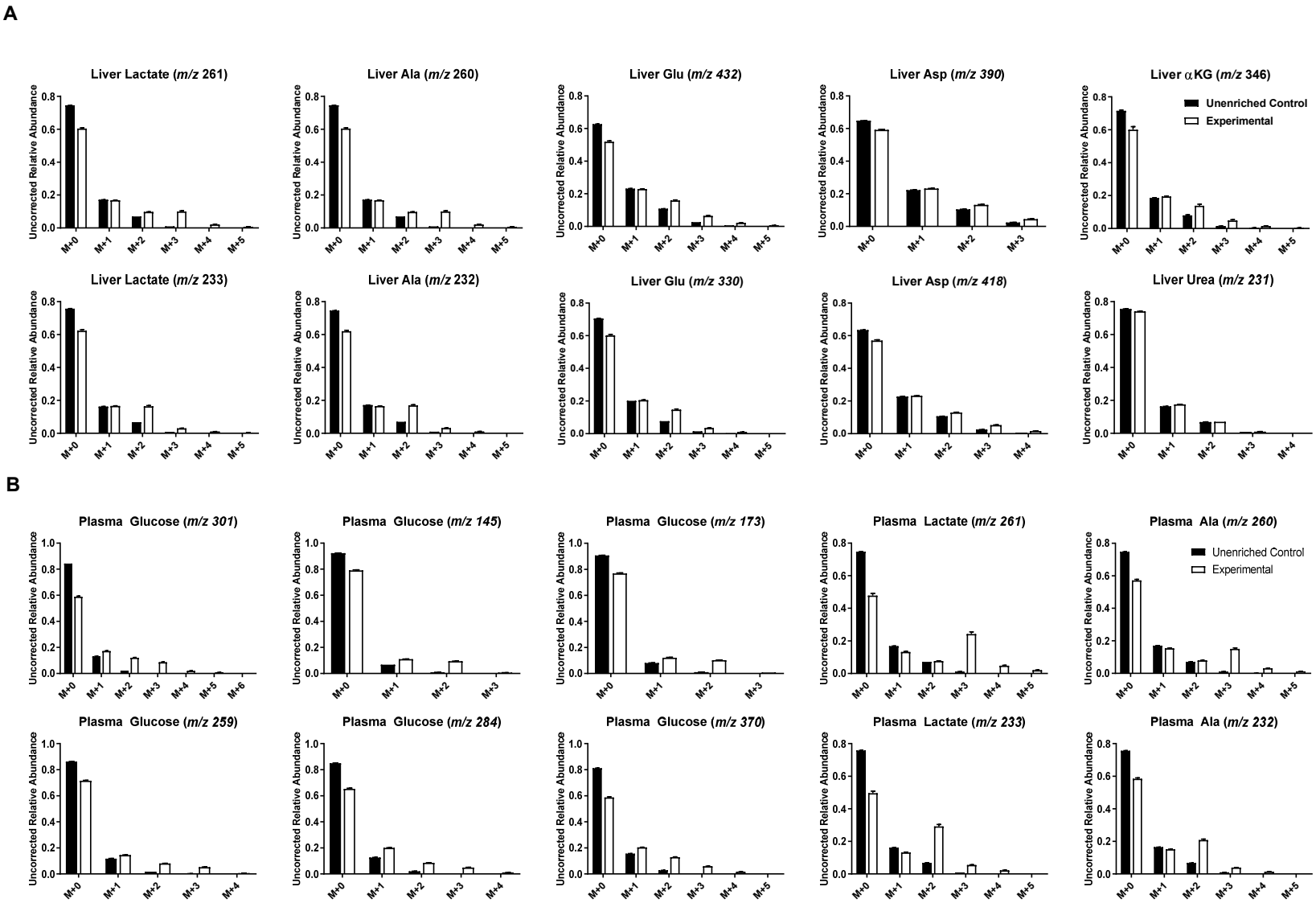

Figure S3. Mass isotopomer measurements for plasma and liver metabolites. Related to Figures 3, 4, S4, S5, S6, and Tables S3 and S5.

(A) Liver lactate (*m/z* 261, 233), alanine (*m/z* 260, 232), glutamate (*m/z* 432, 330), aspartate (*m/z* 418, 390), α-ketoglutarate (*m/z* 346), and urea (*m/z* 231) derivative measurements

(B) Plasma glucose (*m/z* 301,145,173, 259, 284, 370), alanine, (*m/z* 260, 232) and lactate (*m/z* 261, 233) derivative measurements

Enriched mass isotopomer distributions were determined using GC-MS for metabolites extracted from liver and plasma harvested at the close of the experimental period from 19-20hr fasted C57Bl/6J mice infused with $^{13}C_3$Lac. Unenriched samples were obtained from control C57Bl/6 mice for metabolite identification and measurement error determination. Data are presented as means ± SEM (n=7)

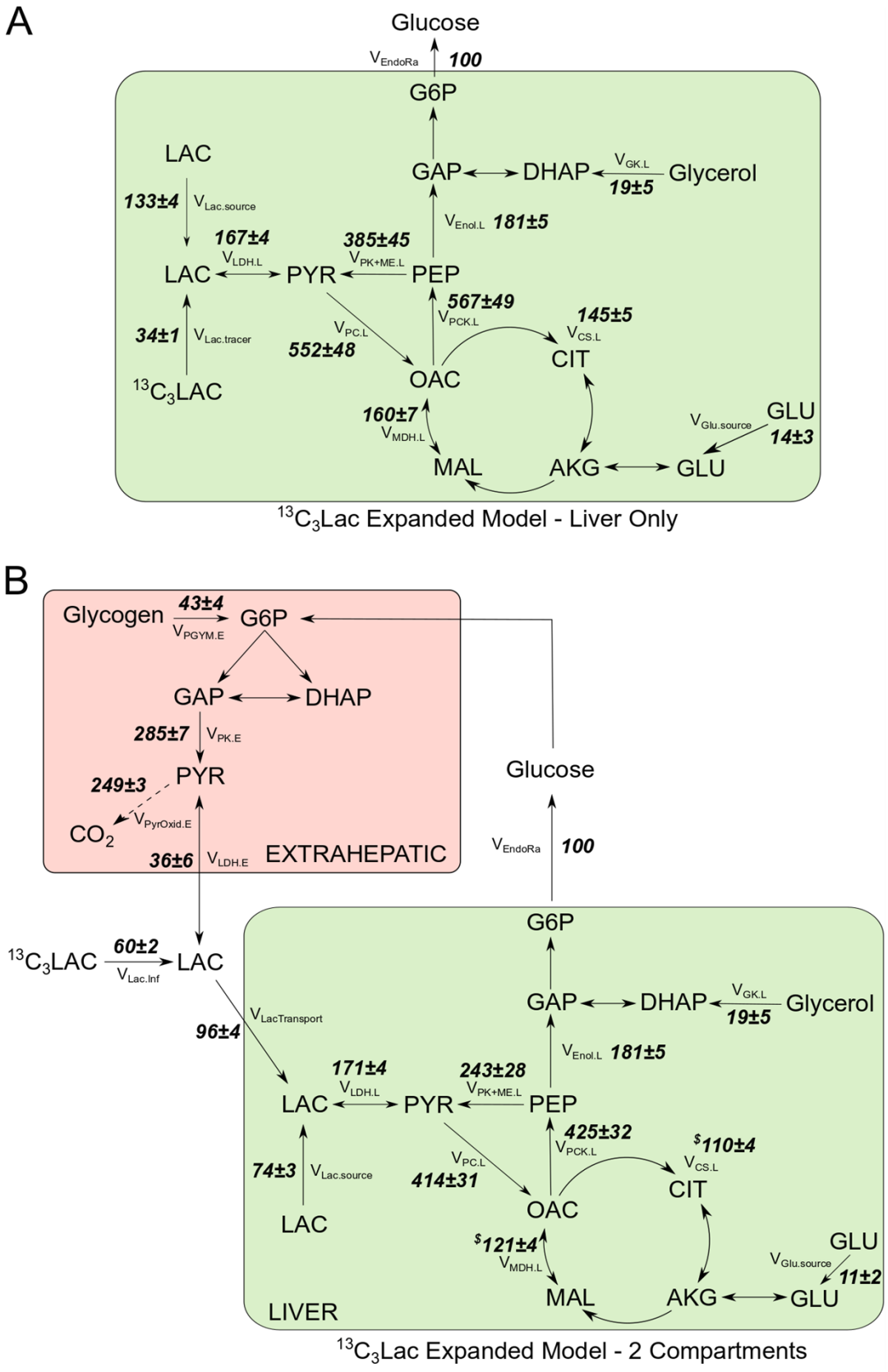

Figure S4. Expansion of models in mice infused with $^{13}C_3$Lac. Related to Figures 4, S3, S5 and Tables S3 and S5

(A) Relative flux estimates from expanded model (liver only) using plasma and liver tissue measurements

(B) Relative flux estimates from the same mice presented in (A) regressed using an expanded model including an extrahepatic compartment to facilitate descriptions of Cori cycling; mice were infused with $^{13}C_3$Lac only.

Data are presented as means ± SEM (n=7) *p<0.05 vs. $^{13}C_3$Lac expanded model – liver only

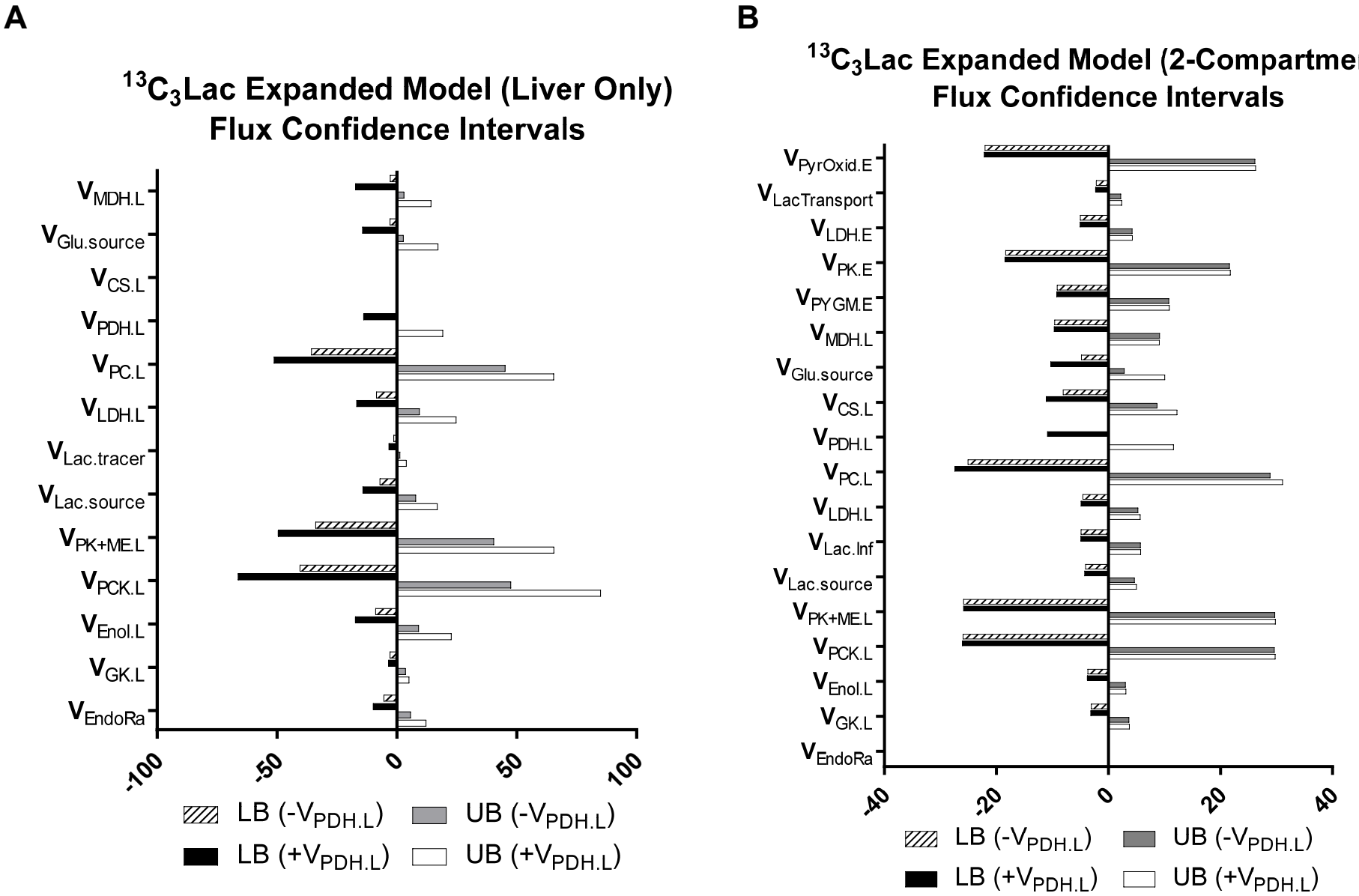

Figure S5. Confidence interval widths in $^{13}C_3$Lac studies. Related to Figures 4, S4 and S6

(A) $^{13}C_3$Lac expanded model – Liver Only for networks without PDH (SSR Ave: 65.1±8.9, Expected Range: 44.6-89.2, DOF: 65) or with PDH (+$V_{PDH.L}$) (SSR Ave: 53.9±6.0, Expected Range 43.8-88, DOF: 64)

(B) $^{13}C_3$Lac expanded model with two compartments for networks without PDH (SSR Ave: 80.7±9.6, Expected Range: 63.1-114.7, DOF: 87) or with PDH (+$V_{PDH.L}$) (SSR Ave: 68.4±6.6, Expected Range: 62.2-113.5, DOF: 86)

Upper and lower bounds are presented as the mean differences (x-axis) from relative flux estimates (n=5-7). Ranges are expressed relative to $V_{CS.L}$=100. The Expected Range of the SSR is calculated from the 95% confidence limits of a chi-square cumulative distribution function with the indicated degrees of freedom (DOF)

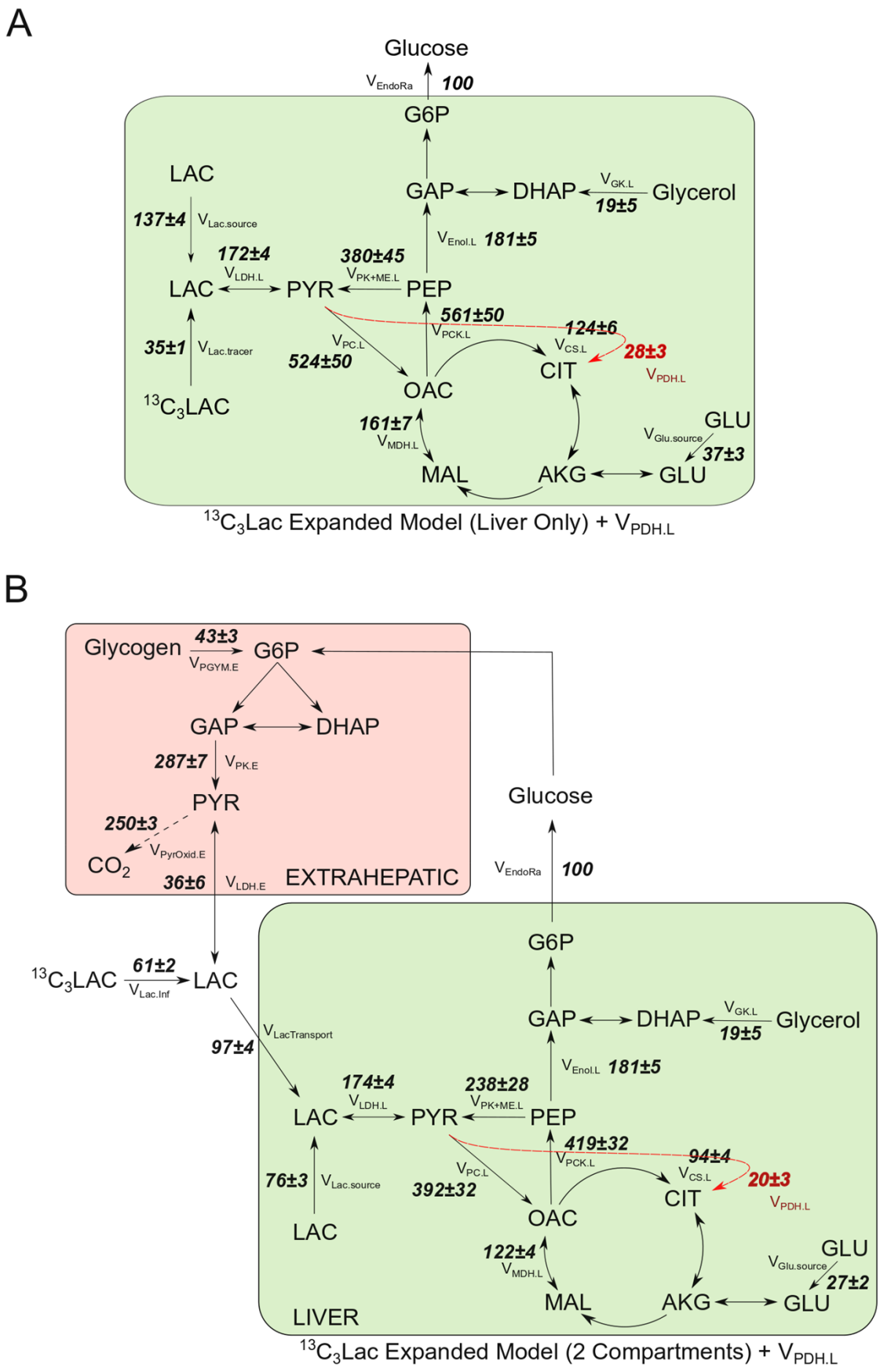

Figure S6. Testing the assumption of low $V_{PDH.L}$ flux during fasting with $^{13}C_3$Lac. Related to Figure 4B, S3, S5, and Tables S3 and S5

(A) Relative flux estimates from expanded model (liver only) using plasma and liver tissue measurements and an active pyruvate dehydrogenase complex (+$V_{PDH.L}$) in the liver

(B) Relative flux estimates from the same mice presented in (A) using a two-compartment expanded model with an active pyruvate dehydrogenase complex (+$V_{PDH.L}$) in the liver

Data are presented as means ± SEM (n=7)

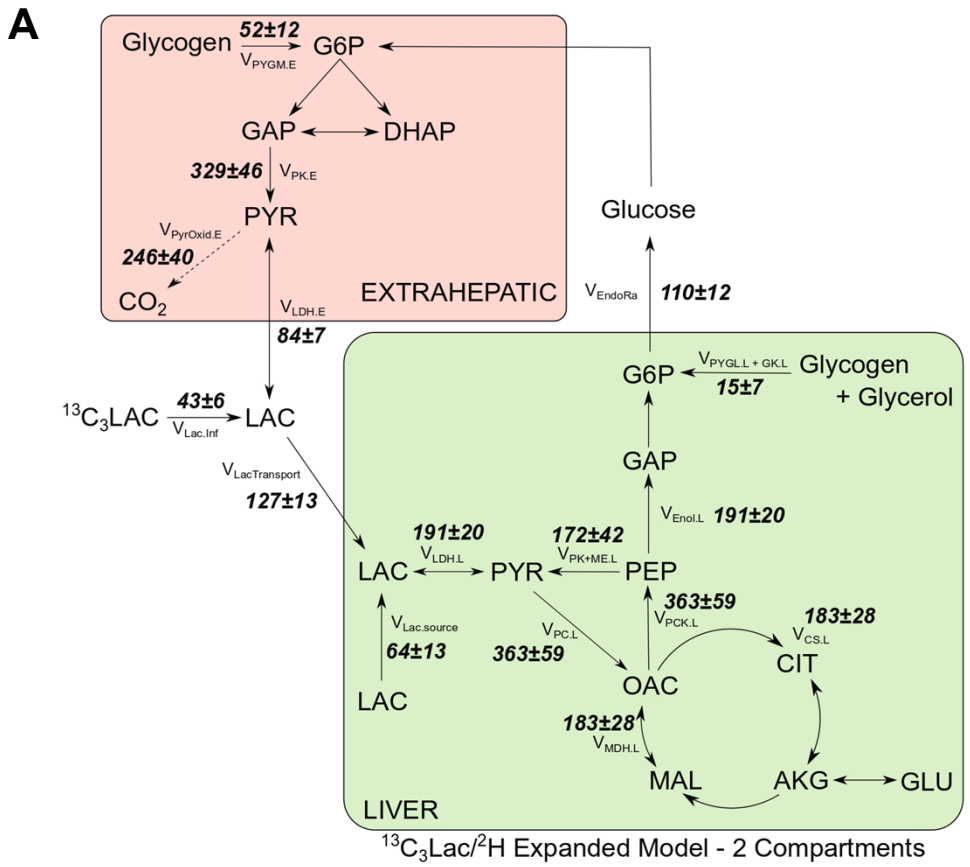

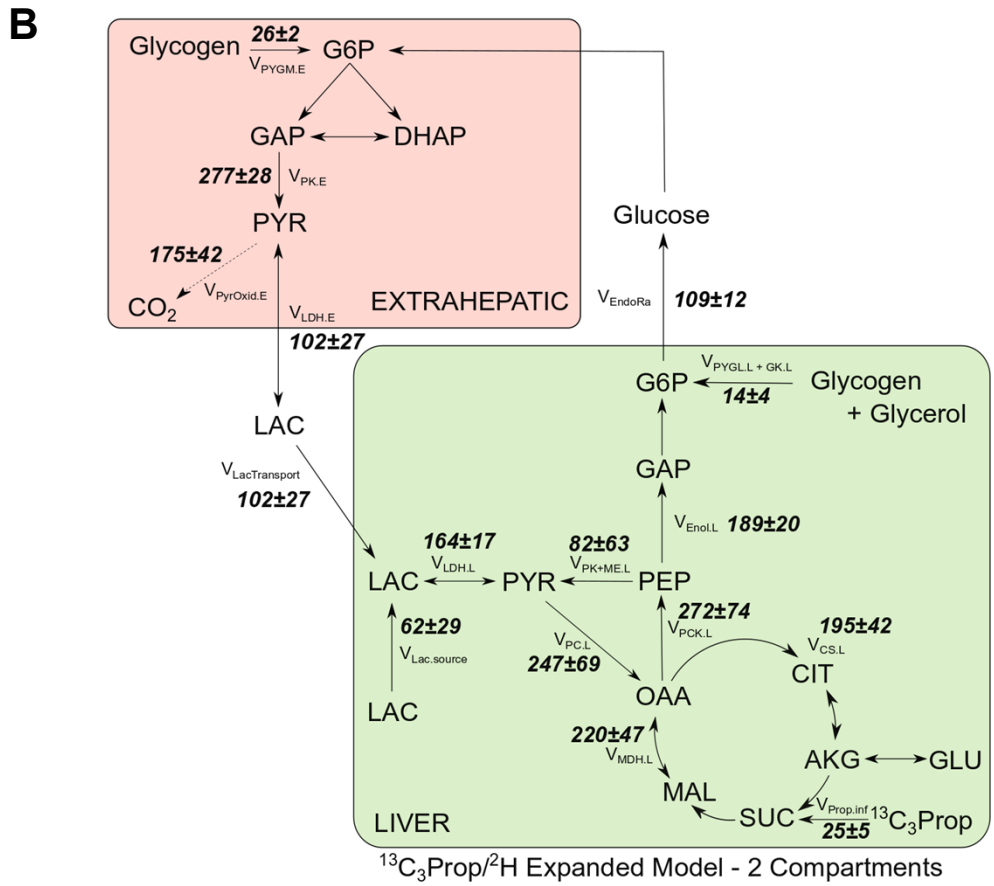

Figure S7. Comparison of $^{13}C_3$Lac/^{2}H and $^{13}C_3$Prop/^{2}H isotopes for hepatic flux estimates using expanded models of metabolism. Related to Figures 5, S2, and Tables S2 and S4

(A) Expanded model (two compartments) showing absolute flux estimates in 19-20hr fasted, C57Bl/6J mice infused with $^{13}C_3$Lac/^{2}H or

(B) $^{13}C_3$Prop/^{2}H isotopes

Data are presented as means ± SEM (µmol/kg/min, n=5)

Flux	Base Model Reaction Network
	Liver Compartment: Glucose Synthesizing and Oxidative Metabolic Reactions
$V_{Glc.inf}$	Glucose.inf (AaBbCcDdEeFfg) → Glucose.P (AaBbCcDdEeFfg)
V_{EndoRa}	H6P (AaBbCcDdEeFfg) → Glucose.P (AaBbCcDdEeFfg)
$V_{PYGL.L}$	Glycogen (AaBbCcDdEeFfg) + H (h) → H6P (AaBhCcDdEeFfg) + H (b)
$V_{Aldo.L}$	T3P (ChBcAab) + T3P (DdEeFfg) + H (i) → H6P (AbBiCcDdEeFfg) + H (h) + H (a)
$V_{GAPDH.L}$	BPG (ABbCcd) + H (e) + H (f) → T3P (AfBeCcd) + H (b)
$V_{GK.L}$	Glycerol (AaeBbCcd) + H (f) → T3P (AeBfCcd) + H (a) + H (b)
$V_{Enol.L}$	PEP (ABCcd) + H (b) → BPG (ABbCcd)
$V_{PK+ME.L}$	PEP (ABCab) + H (c) → Pyr (ABCabc)
$V_{LDH.L}$	Lac (ABbCcde) → Pyr (ABCcde) + H (b)
$V_{Lac.source}$	Lac.source (ABaCbcd) → Lac (ABaCbcd)
$V_{PC.L}$	Pyr (ABCcde) + CO2 (D) + H (f) + H (g) → 0.5*Oac (ABCfgD) + 0.5*Oac (DCBfgA) + H (c)
$V_{PCK.L}$	Oac (ABCabD) → PEP (ABCab) + CO2 (D)
$V_{CS.L}$	Oac (ABCcdD) + AcCoA (EFfgh) → Cit (DCcdBFfgEA) + H (h)
$V_{IDH.L}$	Cit (ABabCDcdEF) + H (e) → Akg (ABCeaDcdE) + H (b) + CO2 (F)
$V_{OGDH.L}$	Akg (ABCabDcdE) → SucCoA (BCabDcdE) + CO2 (A)
$V_{SDH.L}$	SucCoA (ABabCcdD) + H (e) + H (f) → 0.5*Oac (ABCefD) + 0.5*Oac (DCBefA) + H (a) + H
$V_{PCC.L}$	PropCoA (ABabCcde) + CO2 (D) → SucCoA (ACcdBabD) + H (e)
$V_{Bicarb.source}$	Bicarb.source (A) → CO2 (A)
$V_{Bicarb.sink}$	CO2 (A) → Bicarb.sink (A)
$V_{H.inf}$	H.inf (a) → H (a)
$V_{H.sink}$	H → H.sink
	^{13}C-Isotope Infusate Reactions
$V_{Lac.tracer}$	Lac.tracer (ABaCbcd) → Lac (ABaCbcd)
$V_{Prop.tracer}$	Prop.tracer (ABabCcde) → PropCoA (ABabCcde)

Table S1. Base reaction network for ^{2}H/^{13}C MFA. Related to Figures 2D, 2E and S1. The base model of liver metabolism tracks carbon (uppercase) and hydrogen (lowercase) atoms through the specified enzymatic reactions. Fluxes are regressed from plasma measurements of glucose MIDs using either $^{13}C_3$Lac/^{2}H or $^{13}C_3$Prop/^{2}H isotopes. Unenriched sources and sinks are denoted ".source" and ".sink", respectively. ^{2}H and ^{13}C isotopes are introduced into model reactions as ".tracer" sources. Compartments are denoted by ".P" for plasma and ".L" for liver. Liver is the default compartment if no compartment is designated for a metabolite. Simulations were performed post hoc from fluxes regressed to experimental labeling data. Unless otherwise noted here, reaction network and model assumptions have been described elsewhere (Hasenour et al., 2015)

Flux Reaction	Base Model $^{13}C_3$Lac/^{2}H	Base Model $^{13}C_3$Prop/^{2}H	Expanded Model $^{13}C_3$Lac/^{2}H	Expanded Model $^{13}C_3$Prop/^{2}H
$V_{CS.L}$	73 ± 6	100 ± 11	183 ± 28 [b]	195 ± 42
$V_{Enol.L}$	131 ± 16	131 ± 11	191 ± 20	189 ± 20
$V_{PYGL+GK.L}$	26 ± 4	29 ± 3	15 ± 7	14 ± 4
$V_{LDH.L}$	131 ± 16	106 ± 10	191 ± 20	164 ± 17
$V_{PC.L}$	141 ± 19	214 ± 22 [a]	363 ± 59 [b]	247 ± 69
$V_{PCK.L}$	141 ± 19	240 ± 22 [a]	363 ± 59 [b]	272 ± 74
$V_{PK+ME.L}$	9 ± 5	109 ± 13 [a]	172 ± 42 [b]	82 ± 63

Table S2. Comparison of selected flux estimates between base and expanded models of $^{13}C/^{2}H$ studies. Related to Figures 2 and 5, S1 and 7. [a] denotes fluxes that are significantly different between the $^{13}C_3$Lac/^{2}H and $^{13}C_3$Prop/^{2}H Base Models. [b] denotes fluxes that are significantly different between the $^{13}C_3$Lac/^{2}H Base and $^{13}C_3$Lac/^{2}H Expanded Models. Data presented as means (μmol/kg/min) ± SEM ($p \leq 0.05$, n=5-7)

Flux	Expanded Model Reaction Network (^{13}C transitions only)
	Liver Compartment: Glucose Synthesizing and Oxidative Metabolic Reactions
V_{EndoRa}	G6P (ABCDEF) → Glucose.P (ABCDEF)
$V_{Aldo.L}$	DHAP (ABC) + GAP (DEF) → G6P (CBADEF)
$V_{TPI.L}$	DHAP (ABC) ←→ GAP (ABC)
$V_{GAPDH.L}$	BPG (ABC) → GAP (ABC)
$V_{GK.L}$	Glycerol (ABC) → DHAP (ABC)
$V_{Enol.L}$	PEP (ABC) → BPG (ABC)
$V_{PK+ME.L}$	PEP (ABC) → Pyr (ABC)
$V_{LDH.L}$	Lac (ABC) ←→ Pyr (ABC)
$V_{Lac.source}$	Lac.source (ABC) → Lac (ABC)
$V_{ALT.L}$	Ala (ABC) ←→ Pyr (ABC)
$V_{PC.L}$	Pyr (ABC) + CO2 (D) → Oac (ABCD)
$V_{PCK.L}$	Oac (ABCD) → PEP (ABC) + CO2 (D)
$V_{PDH.L}$	Pyr (ABC) → AcCoA (BC) + CO2 (A)
$V_{\beta Oxid.L}$	Fat (AB) → AcCoA (AB)
$V_{CS.L}$	Oac (ABCD) + AcCoA (EF) → Cit (DCBFEA)
$V_{IDH.L}$	Cit (ABCDEF) ←→ Akg (ABCDE) + CO2 (F)
$V_{GDH.L}$	Glu (ABCDE) ←→ Akg (ABCDE)
$V_{Glu.source}$	Glu.source (ABCDE) → Glu (ABCDE)
$V_{OGDH.L}$	Akg (ABCDE) → SucCoA (BCDE) + CO2 (A)
$V_{SCS.L}$	SucCoA (ABCD) → Suc* (ABCD)
$V_{SDH.L}$	Suc* (ABCD) ←→ Fum* (ABCD)
$V_{FH.L}$	Fum* (ABCD) ←→ Mal (ABCD)
$V_{MDH.L}$	Mal (ABCD) ←→ Oac (ABCD)
$V_{Bicarb\ source}$	Bicarb.source (A) → CO2 (A)
$V_{Bicarb\ sink}$	CO2 (A) → Bicarb.sink (A)
	^{13}C-Isotope Infusate Reactions
$V_{Lac.tracer}$	Lac.inf (ABC) → Lac (ABC)
$V_{Lac.inf}$	Lac.inf (ABC) → Lac.P (ABC)

Table S3. Expanded reaction network for ^{13}C MFA. Related to Figures 4, S4 and S6. (Table and caption continues to next page)

Extrahepatic Compartment: Glycolytic, and Cori Cycle Reactions	
$V_{HK.E}$	Glucose.P (ABCDEF) → G6P.E (ABCDEF)
$V_{PYGM.E}$	Glycogen.E (ABCDEF) → G6P.E (ABCDEF)
$V_{Aldo.E}$	G6P.E (ABCDEF) → GAP.E (CBA) + DHAP.E (DEF)
$V_{TPI.E}$	GAP.E (ABC) ←→ DHAP.E (ABC)
$V_{GAPDH.E}$	GAP.E (ABC) → BPG.E (ABC)
$V_{Enol.E}$	BPG.E (ABC) → PEP.E (ABC)
$V_{PK.E}$	PEP.E (ABC) → Pyr.E (ABC)
$V_{PyrOxid.E}$	Pyr.E (ABC) → CO2 (A) + CO2 (B) + CO2 (C)
$V_{LDH.E}$	Pyr.E (ABC) ←→ Lac.P (ABC)
$V_{LacTransport}$	Lac.P (ABC) → Lac (ABC)

Table S3 (Continued). Expanded reaction network for ^{13}C MFA. Related to Figures 4, S4 and S6. Expanded model of liver metabolism for tracking only carbon atoms through the specified enzymatic reactions. Fluxes are regressed from liver and plasma measurements for mice infused with $^{13}C_3$Lac. Unenriched sources and sinks are denoted ".source" and ".sink", respectively. Infused ^{13}C isotopes are introduced into model reactions as ".tracer" sources in liver-only models or ".inf" sources for two-compartment models. (Note that these two types of tracer input fluxes are not expected to be equivalent in the case of $^{13}C_3$Lac administration, since $V_{Lac.tracer}$ represents liver-specific uptake of the tracer while $V_{Lac.inf}$ represents infusion of tracer into the plasma compartment.) Compartments are denoted by ".P" for plasma, ".E" for extrahepatic, and ".L" for liver. Liver is the default compartment if no compartment is designated for a metabolite. The two-compartment model includes reactions for the liver, ^{13}C-bicarbonate recycling, and Cori cycle reactions. *denotes that the carbons of succinate and fumarate are symmetric

Flux	Expanded Model Reaction Network ($^{2}H/^{13}C$ transitions)
	Expanded Liver Compartment: Glucose Synthesizing and Oxidative Metabolic Reactions
$V_{Glc.Inf}$	Glucose.inf (AaBbCcDdEeFfg) → Glucose.P (AaBbCcDdEeFfg)
V_{EndoRa}	G6P (AaBbCcDdEeFfg) → Glucose.P (AaBbCcDdEeFfg)
$V_{PYGL.L}$	Glycogen (AaBbCcDdEeFfg) + H (h) → G6P (AaBhCcDdEeFfg) + H (b)
$V_{Aldo.L}$	DHAP (AabBCcd) + GAP (DeEfFgh) + H (i) → G6P (CdBiAaDeEfFgh) + H (b) + H (c)
$V_{TPI.L}$	DHAP (AabBCcd) + H (e) ←→ GAP (AbBeCcd) + H (a)
$V_{GAPDH.L}$	BPG (ABbCcd) + H (a) → GAP (AaBbCcd)
$V_{GK.L}$	Glycerol (AabBeCcd) → DHAP (AabBCcd) + H (e)
$V_{Enol.L}$	PEP (ABCcd) + H (b) → BPG (ABbCcd)
$V_{PK+ME.L}$	PEP (ABCab) + H (c) → Pyr (ABCabc)
$V_{LDH.L}$	Lac (ABbCcde) ←→ Pyr (ABCcde) + H (b)
$V_{Lac.source}$	Lac.source (ABbCcde) → Lac (ABbCcde)
$V_{ALT.L}$	Ala (ABbCcde) + H (f) ←→ Pyr (ABCcdf) + H (b) + H (e)
$V_{PC.L}$	Pyr (ABCcde) + CO2 (D) → Oac (ABCcdD) + H (e)
$V_{PCK.L}$	Oac (ABCabD) → PEP (ABCab) + CO2 (D)
$V_{CS.L}$	Oac (ABCcdD) + AcCoA (EFfgh) → Cit (DCcdBFfgEA) + H (h)
$V_{IDH.L}$	Cit (ABabCDcdEF) + H (e) ←→ Akg (ABCeaDcdE) + H (b) + CO2 (F)
$V_{GDH.L}$	Glu (ABeCabDcdE) ←→ Akg (ABCabDcdE) + H (e)
$V_{OGDH.L}$	Akg (ABCabDcdE) → SucCoA (BCabDcdE) + CO2 (A)
$V_{SCS.L}$	SucCoA (ABabCcdD) → Suc* (ABabCcdD)
$V_{PCC.L}$	PropCoA (ABabCcde) + CO2 (D) → SucCoA (ACcdBabD) + H (e)
$V_{SDH.L}$	Suc* (ABabCcdD) ←→ Fum* (ABaCdD) + H (b) + H (c)
$V_{FH.L}$	Fum* (ABaCbD) + H (c) ←→ Mal (ABaCcbD)
$V_{MDH.L}$	Mal (ABaCbcD) ←→ Oac (ABCbcD) + H (a)
$V_{Bicarb.source}$	Bicarb.source (A) → CO2 (A)
$V_{Bicarb.sink}$	CO2 (A) → Bicarb.sink (A)
$V_{H.inf}$	H.inf (a) → H (a)
$V_{H.sink}$	H → H.sink

Table S4. Expanded reaction network for $^{2}H/^{13}C$ MFA. Related to Figures 5 and S7. (Table and caption continues to next page)

	^{13}C-Isotope Infusate Reactions
$V_{Lac.inf}$	Lac.inf (ABbCcde) → Lac.P (ABbCcde)
$V_{Prop.inf}$	Prop.inf (ABabCcde) → PropCoA (ABabCcde)

	Expanded Extrahepatic Compartment: Glycolytic, and Cori Cycle Reactions
$V_{HK.E}$	Glucose.P (AaBbCcDdEeFfg) → G6P.E (AaBbCcDdEeFfg)
$V_{PYGM.E}$	Glycogen.E (AaBbCcDdEeFfg) + H (h) → G6P.E (AaBhCcDdEeFfg) + H (b)
$V_{Aldo.E}$	G6P.E (CdBiAaDeEfFgh) + H (b) + H (c) → DHAP.E (AabBCcd) + GAP.E (DeEfFgh) + H (i)
$V_{TPI.E}$	DHAP.E (AabBCcd) + H (e) ←→ GAP.E (AbBeCcd) + H (a)
$V_{GAPDH.E}$	GAP.E (AaBbCcd) → BPG.E (ABbCcd) + H (a)
$V_{Enol.E}$	BPG.E (ABbCcd) → PEP.E (ABCcd) + H (b)
$V_{PK.E}$	PEP.E (ABCab) + H (c) → Pyr.E (ABCabc)
$V_{ALT.E}$	Ala.E (ABbCcde) + H (f) ←→ Pyr.E (ABCcdf) + H (b) + H (e)
$V_{PyrOxid.E}$	Pyr.E (ABCcde) → H (c) + H (d) + H (e) + CO2 (A) + CO2 (B) + CO2 (C)
$V_{LDH.E}$	Pyr.E (ABCcde) + H (b) ←→ Lac.P (ABbCcde)
$V_{LacTransport}$	Lac.P (ABbCcde) → Lac (ABbCcde)

Table S4 (Continued). Expanded reaction network for ^{2}H/^{13}C MFA. Related to Figures 5 and S7. Expanded model of liver metabolism for tracking both carbon (uppercase) and hydrogen (lowercase) atoms through the specified enzymatic reactions. Fluxes are regressed from liver and plasma measurements using either $^{13}C_3$Lac/^{2}H or $^{13}C_3$Prop/^{2}H isotopes. See Tables S1 and S3 for nomenclature

Metabolite	m/z	Formula	Carbons
Alanine	260	$C_{11}H_{26}O_2NSi_2$	1 2 3
Alanine	232	$C_{10}H_{26}ONSi_2$	2 3
Aspartate	390	$C_{17}H_{40}O_3NSi_3$	2 3 4
Aspartate	418	$C_{18}H_{40}O_4NSi_3$	1 2 3 4
α-Ketoglutarate	346	$C_{14}H_{28}O_5NSi_2$	1 2 3 4 5
Glutamate	432	$C_{19}H_{42}O_4NSi_3$	1 2 3 4 5
Glutamate	330	$C_{16}H_{36}O_2NSi_2$	2 3 4 5
Glucose	370	$C_{17}H_{24}O_8N$	1 2 3 4 5
Glucose	301	$C_{14}H_{21}O_7$	1 2 3 4 5 6
Glucose	284	$C_{13}H_{18}O_6N$	1 2 3 4
Glucose	259	$C_{12}H_{19}O_6$	4 5 6
Glucose	173	$C_8H_{13}O_4$	5 6
Glucose	145	$C_6H_{11}O_3N$	1 2
Lactate	261	$C_{11}H_{25}O_3Si_2$	1 2 3
Lactate	233	$C_{10}H_{25}O_2Si_2$	2 3
Urea	231	$C_9H_{23}N_2OSi_2$	1

Table S5. Measured GC-MS fragment ions. Related to all Figures.